New archeointensity data from French Early Medieval pottery production (6th–10th century AD). Tracing 1500 years of geomagnetic field intensity variations in Western Europe

Agnès Genevey, Yves Gallet, Sébastien Jesset, Erwan Thébault, Jérôme Bouillon, Annie Lefèvre, Maxime Le Goff

New Archeointensity Data from French Early Medieval Pottery Production (6th-10th century AD). Tracing 1500 years of Geomagnetic Field Intensity Variations in Western Europe.

Agnès Genevey[1], Yves Gallet[2], Sébastien Jesset[3], Erwan Thébault[4], Jérôme Bouillon[5], Annie Lefèvre[6], Maxime Le Goff[2]

[1]Sorbonne Universités, UPMC Univ Paris 06, CNRS, UMR 8220, Laboratoire d'archéologie moléculaire et structurale (LAMS), 4 place Jussieu 75005 Paris, France, corresponding author

[2]Institut de Physique du Globe de Paris- Sorbonne Paris Cité- Université Paris Diderot, UMR 7154 CNRS, Paris, France.

[3]Mairie d'Orléans, Service Archéologique Municipal d'Orléans, Orléans, France.

[4]Université de Nantes, LPG UMR-CNRS 6112- Laboratoire de Planétologie et Géodynamique de Nantes, Nantes, France.

[5]Institut National de Recherches Archéologiques Préventives, Centre de recherches archéologiques de Tours, Tours, France.

[6]Institut National de Recherches Archéologiques Préventives, Centre de recherches archéologiques de la Courneuve, La Courneuve, France.

Highlights

- 19 French archeointensity data are obtained from groups of Early Medieval potsherds
- An experimental pottery firing asserts the reliability of the Triaxe protocol
- A Western European intensity variation curve is constructed for the past 1500 years
- A sequence of 5 intensity maxima is observed with a recurrence of ~250 years

Keywords

Archeointensity, Geomagnetic Secular Variation, Medieval Period, Western Europe, Experimental Archeological Firing, Pottery

Abstract

Nineteen new archeointensity results were obtained from the analysis of groups of French pottery fragments dated to the Early Middle Ages (6th to 10th centuries AD). They are from several medieval ceramic production sites, excavated mainly in Saran (Central France), and their precise dating was established based on typo-chronological characteristics. Intensity measurements were performed using the Triaxe protocol, which takes into account the effects on the intensity determinations of both thermoremanent magnetization anisotropy and cooling rate. Intensity analyses were also carried out on modern pottery produced at Saran during an experimental firing. The results show very good agreement with the geomagnetic field intensity directly measured inside and around the kiln, thus reasserting the reliability of the Triaxe protocol and the relevance of the quality criteria used. They further demonstrate the potential of the Saran pottery production for archeomagnetism. The new archeointensity results allow a precise and coherent description of the geomagnetic field intensity variations in Western Europe during the Early Medieval period, which was until now poorly documented. They show a significant increase in intensity during the 6th century AD, high intensity values from the 7th to the 9th century, with a minimum of small amplitude at the transition between the 7th and the 8th centuries and finally an important decrease until the beginning of the 11th century. Together with published intensity results available within a radius of 700 km around Paris, the new data were used to compute a master curve of the Western European geomagnetic intensity variations over the past 1500 years. This curve clearly exhibits five intensity maxima: at the transition between the 6th and 7th century AD, at

the middle of the 9th century, during the 12th century, in the second part of the 14th century and at the very beginning of the 17th century AD. Some of these peaks are smoothed, or nearly absent when the selection of the data is extended to a 1250 km radius around Paris. The apparent regularity in the occurrence of intensity maxima, with a recurrence of ~250 years, is particularly intriguing and might reflect a new characteristic of the secular variation, at least in Western Europe. It clearly requires further investigation and in particular the acquisition of new data from older periods.

Introduction

The Early Middle Ages in Western Europe spanned from the end of the 5th century to the beginning of the 11th century AD (e.g. Devroey, 2003; Davis, 2005). The perception of this period, often called the "Dark Ages", has largely been re-evaluated in France over the past 20 years thanks to rescue archeology. Numerous archeological excavations conducted during the re-development within towns and in the countryside have enabled a better understanding of the medieval habitat and of everyday life. This new information has revealed a less abrupt transition period after the fall of the Roman Empire (e.g. Catteddu, 2009). Furthermore, these excavations have offered unique opportunities for studying the geomagnetic secular variation during this time interval. In particular, a large set of domestic kilns was sampled for archeomagnetic directional analyses in the Ile-de-France region, near Paris (Warmé, 2009) and the new results aim to contribute to the refinement of the French directional variation curve during the Middle Ages. The discovery of pottery workshops, ranging from small units to large production centers, also provided material for archeomagnetic directional and/or intensity studies.

The need for new archeointensity results from the Early Middle Ages has long been recognized (e.g. Chauvin et al., 2000; Genevey and Gallet, 2002). Despite recent and

78 significant improvements (Donadini et al., 2008, 2012; Gallet et al., 2009; Tema et al., 2009;
79 Gómez-Paccard et al., 2012), this period remains poorly documented, which penalizes the
80 construction of accurate regional and/or global archeomagnetic field models (e.g. Pavón-
81 Carrasco et al., 2014a, 2014b). The acquisition of new archeointensity data dated to the Early
82 Middle Ages is thus still necessary in order to build a detailed and continuous geomagnetic
83 field intensity variation curve for Western Europe over the past 2000 years (Genevey et al.,
84 2009, 2013).

85 We present here 19 new archeointensity data dated to the Early Middle Ages, among
86 which 16 were obtained from the analysis of pottery fragments produced at Saran (Fig. 1a).
87 This site, located a few kilometers north of the city of Orléans, France, was an important
88 center of pottery production during the Middle Ages as evidenced by the numerous pottery
89 kilns and associated ceramics found during excavations (Jesset et al., 2001, 2010; Jesset,
90 2013, 2015a,b; Bouillon, 2015). The archeointensity analysis of two groups of potsherds
91 produced in Saran had previously been carried out by Genevey and Gallet (2002). These
92 results are here reassessed in the light of new information provided by an experimental firing
93 conducted on a reconstructed ancient kiln, which allowed a re-estimation of the cooling rate
94 experienced by the ceramics. We further present intensity results obtained from modern
95 pottery produced in known field conditions during this experimental firing.

96

97 **Archeological collection**

98 In the late sixties, when the archeological site of Lac de la Médecinerie was
99 discovered in Saran (47.9°N, 1.9°N; Fig. 1a) and partially excavated (Chapelot, 1973), Emile
100 Thellier sampled the kilns that were unearthed at the time. While being amongst the first
101 structures analyzed in France for their archeomagnetic directions (Thellier, 1981), the Lac de
102 la Médecinerie was the first archeological site revealing a medieval pottery activity in this

city. Since then, other production units have been discovered at Saran and archeological excavations are still being conducted some 40 years later, in particular at the Lac de la Médecinerie site (Jesset et al., 2010). This on-going work has allowed Saran to be recognized as a major center of ceramic production in Central France during the Merovingian (5th-mid 8th century AD) and Carolingian (mid 8th-10th century AD) royal dynasties.

A detailed chrono-typology for the Saran production was constructed by crossing different information (e.g. Jesset, 2013, 2015b). It relies on constraints derived from the excavations conducted at Saran and also on various elements obtained from other sites where ceramics produced at Saran were discovered in a consumer context. These elements include radiocarbon dating, coins and historical constraints among others. The chronology is based on the recognition of the changing characteristics of pottery over time, such as the shape of the ceramics including the evolution of the lips, spout and the base, their function, the color and the texture of the paste, the overall quality of the production and also the decor, here often made with a small wooden wheel. The derived chronology runs from the 6th to the beginning of the 11th century AD. We only summarize below the major evolutionary trends of the ceramics produced at Saran, whose resolution allows dating with a precision of ±25 years in favorable cases. This should not hide the fact that the typo-chronology relies on the identification and integration of more elements than those presented here (Jesset, 2013, 2015b).

The beginning of ceramic production in Saran, during the 5th century AD, remains relatively unknown. Only a few grey shards with polished surfaces, fired in redox conditions and of Gallo-Roman appearance give evidence of some preliminary small-scale production. The 6th century AD is better documented; this period is characterized by forms and decors also inherited from the Gallo-Roman corpus, with thick walls (> 5 mm) and by ochre-yellow clay paste with a light grey color at the core. The 7th century sees the reinforcement of the

production activity and the expansion of its area of distribution, reaching a monopoly position during the early 8th century through a region of 50 to 70 km around Saran. While most technological characteristics of the production do not change during the 7th century AD, such as the texture, the color and the thickness of ceramics, the production tends, however, to become more standardized due to the higher rate of production, with simpler decor and more rounded shapes. In contrast, the 8th century is characterized by significant evolution: the walls become thinner (3 to 4 mm) and the color of the pots darkened to red-ochre. The old forms are abandoned or evolve and new forms emerge. As an example, the trefoil tubular spout, which had appeared at the end of the 7th century, was at first separated from the neck of the pottery before gradually converging with it and finally fusing into it in the second half of the 8th century. A decline in quality of the ceramic production is also perceived during the second half of the 8th century, as evidenced by pots presenting defects discovered in consumer contexts. This decline continues during the 9th century, with a more reduced corpus of production, which foreshadows the end of the main workshops of Saran in the second part of the 9th century. For this period, the evolution of the shapes and of the lips of the globular pots serves as a chronological marker. The color of the ceramics dated to the 9th century is dark at first, before becoming brighter in the late 9th century, with a light ochre-yellow clay paste that characterizes the ceramics of the 10th century. The ceramics at this point are produced in small production units at Saran and the weaker activity likely favors an overall higher quality of the ceramics. Thicker walls are observed and a new profile of lips “en bandeau” appears during the second part of the 10th century, before the generalization of the latter during the 11th century, when, unfortunately, the ceramic production in Saran is no longer documented.

Considering only the groups of potsherds that successfully provided archeointensity results, our collection from Saran is composed of 17 groups encompassing the period from the 6th to the 10th century. They are mostly associated to two important production units excavated

153 at the sites of Lac de la Médecinerie (6 groups) and La Guignace (7 groups), both situated
154 along the old Roman road between Chartres and Orléans. Three other groups consist of
155 pottery fragments from a smaller workshop excavated at the archeological site of Zac des
156 Vergers, which had been in activity during Saran's period of peak production. The last group,
157 dated to the end of the 9th century, was sampled from a large set of ceramic fragments
158 discovered during domestic building works in the current center of Saran (Saran le Bourg).

159 All fragments collected at Saran were found in pits inside or nearby the kilns where
160 they were originally produced. They correspond to pottery wasters that were used to fill in the
161 kilns after their abandonment. The selected fragments (as illustrated in Fig. 1b) are from units
162 with a low level of pottery fragmentation and the potsherds show sharp (rather than eroded)
163 sides. These are good indicators that the fragments were thrown away soon after their
164 production. For each group, the fragments are from one or two stratigraphic units associated
165 to a single filling phase and were chosen to be representative of the ceramic materials, which
166 allow dating of the filling phase. These groups are homogenous in terms of the granularity
167 and color of the clay paste. In only one case, two successive filling events were sampled in
168 one kiln and two distinct groups of potsherds were thus constituted (SAR13 and SAR14). We
169 further note that the groups referred to as A36 and A38 were previously analyzed by Genevey
170 and Gallet (2002). These old results are here reevaluated and group A36 has also benefited
171 from a resampling (SAR08).

172 Sampling at Saran was complemented by other groups of pottery fragments produced
173 elsewhere. A group was collected at Ingré (47.9°N, 1.8°E; Fig. 1a) about 10 km southwest of
174 Saran. This site was a pottery workshop active during the 7th century. The production is
175 characterized by a decor made with a punch, a practice rarely used in Saran. The ceramic
176 corpus is, however, the same as that of Saran and the dating for this group thus relies on the
177 same typo-chronology. Three groups of pottery fragments were also produced in Vanves

178 (48.8°N, 2.3°E), a suburb to the south west of Paris (Fig. 1a). Excavations have revealed that
179 Vanves was a major pottery production center for the region around Paris from the 6th to the
180 9th centuries, as was Saran for the central region of France. Excavations conducted in the
181 street Rue Gaudray, in the historical center of Vanves, enabled the discovery of six pottery
182 kilns close to each other, with several pits filled with failed ceramics (Lefèvre and Peixoto,
183 2015). Archeointensity results were already obtained from this site (Gallet et al., 2009). In the
184 present study, we report on a new set of results from fragments collected in the filling layer in
185 one of the six kilns, which is dated to between the middle of the 7th and the middle of the 8th
186 century. This dating is based on typo-morphological evidence, such as the presence of
187 fragments from large bowls with a small pinched spout and bowls with a wide band, both
188 indicative of the end of the Merovingian period. We also note the presence of bi-conical
189 vases, which were produced during the entire Merovingian period with an evolution over time
190 from a fine, fumigated and polished paste to a granular production; this form then completely
191 disappeared during the 8th century (Lefèvre, 2007). The collected fragments have a coarse
192 paste with medium size inclusions (1 to 1.5 mm) and a color ranging from orange-beige to
193 brown (Fig. 1c). Archeological data from another site (20 Place de la République) close to
194 Rue Gaudray have documented the early medieval pottery production at Vanves, i.e. during
195 the 6th century. No kiln was discovered but the potsherds found in different pits were
196 undoubtedly identified as failed pottery. The shapes of these ceramics are characteristics of
197 the 6th century AD, with flanged or carinated open forms and bi-conical pots (Lefèvre, 2009).
198 Two fragment groups with the very same typo-morphological characteristics (having a coarse
199 paste of light color with fine inclusions of less than 1 mm) and therefore having the same age,
200 were collected from two pits (groups referred to as VAN04 and VAN05) and their
201 archeomagnetic results will be discussed together.
202

Intensity and Rock Magnetic Experiments

All experiments were carried out at the paleomagnetic laboratory of the Institut de Physique du Globe de Paris and the Laboratory of Structural and Molecular Archeology (LAMS) of Pierre et Marie Curie University, Paris. Intensity measurements were performed using Triaxe magnetometers (Le Goff and Gallet, 2004). The experimental protocol, derived from the Thellier and Thellier (1959) method, has been extensively described in previous studies (e.g. Gallet and Le Goff, 2006; Genevey et al., 2009; Hartmann et al., 2010) and we here present below only its key features and the main steps.

The Triaxe protocol involves continuous high-temperature magnetization measurements of a small specimen of ~1cm in height and with a thickness depending on that of the fragment. It comprises a series of heating and cooling steps. In the first step, the Natural Remanent Magnetization (NRM) of the specimen is demagnetized between a low temperature T1 fixed at 150°C and a high temperature T2, here fixed between 480°C and 530°C depending on the specimen. After the determination of the thermal variation between T1 and T2 of the NRM fraction still blocked above T2, a thermoremanent magnetization (TRM) is acquired by cooling down the specimen from T2 to T1 in a laboratory field whose intensity is chosen close to the expected value. The direction of the field is also adjusted in order to produce a TRM parallel to the NRM direction, which allows one to account for the TRM anisotropy effect (Le Goff and Gallet, 2004). This laboratory TRM is demagnetized by heating again the specimen from T1 to T2. From these different series of measurements, the ratios between the NRM and TRM fractions demagnetized between T1 and a running temperature Ti, every 5°C, from T1 to T2 are computed and multiplied by the intensity of the laboratory field to obtain the R'(Ti) data (see in Le Goff and Gallet, 2004). The R'(Ti) data are finally averaged between T1 and T2 to obtain an archeointensity value at the specimen level. When a secondary magnetization component is observed above T1, the computations

228 are performed over a reduced temperature interval (between T1' and T2) where only the
229 primary TRM is demagnetized. Interestingly, as the Triaxe allows the acquisition of an almost
230 full TRM in the same way as the NRM (instead of partial TRMs as in more classical intensity
231 methods), the protocol limits the impact of the possible presence of multidomain grains on
232 intensity determination. Furthermore, it was experimentally observed from analyses on a large
233 collection of fragments that the Triaxe protocol allows overcoming the cooling rate effect on
234 TRM acquisition (Le Goff and Gallet, 2004; Genevey et al., 2009; Hartmann et al., 2010,
235 2011).

236 The intensity determinations were evaluated through a set of quality criteria identical
237 to those used in previous studies (for example Genevey et al., 2009). In particular, at the
238 specimen level, the R'(Ti) data are averaged on a temperature interval over which only the
239 primary magnetization component is isolated and which involves more than 50% of the
240 magnetization remaining above the chosen temperature T1/T1', while the slope defined by the
241 R'(Ti) values must be of less than 10%. The coherence of the intensity determinations is first
242 tested from the analysis of two to three specimens per fragment, with an error in the mean
243 intensity calculated at the fragment level that must be lower than 5%. A minimum of three
244 intensity values determined at the fragment level (with fragments collected from different
245 pots) is required to define a mean intensity value at the group level and the standard deviation
246 of the latter must be lower than 10% and lower than 5μT. It is worth recalling that the
247 reliability of the Triaxe protocol and the pertinence of the applied quality criteria have been
248 tested from cross comparison between intensity results obtained using classical intensity
249 methods, with strict quality criteria, and the Triaxe procedure (Genevey et al., 2009;
250 Hartmann et al., 2010, 2011). Nevertheless, the experimental firing performed in Saran, with
251 modern pots produced in controlled thermal and magnetic field conditions, provided the

252 opportunity to further attest to the reliability of the Triaxe archeointensity data and to offer
253 new insights into the cooling rate effect.

254 In addition to the behavior observed during the Triaxe measurements, the stability of
255 the magnetic mineralogy on heating, i.e. a basic request for intensity experiments, was also
256 systematically tested through the reversibility of the heating and cooling curves of the low
257 field magnetic susceptibility obtained using a KLY3 Kappabridge coupled with a CS3
258 furnace. In most cases, the maximum temperature for these experiments has been fixed at
259 500°C because the NRM of the specimens is generally completely or almost completely
260 demagnetized at this temperature.

261 For characterizing the magnetic mineralogy of the studied fragments, thermomagnetic
262 susceptibility measurements were carried out up to ~680°C on two fragments from each
263 group. Further investigations were conducted on fresh specimens by the acquisition of
264 Isothermal Remanent Magnetization (IRM) curves in fields up to a maximum of ~1T and of
265 hysteresis loops using a Vibrating Sample Magnetometer (VSM). Thermal demagnetization
266 of three-axis IRM (1.25T, 0.4T, and 0.2T) acquired along three perpendicular directions
267 (Lowrie, 1990) was also performed on one fragment from each group, the ensemble reflecting
268 the variability of the magnetic mineralogy. Finally, IRM acquisition up to 9T was conducted
269 using a Magnetic Measurement Pulse Magnetizer MMPM10 on a set of six fragments
270 selected according to the three-axis IRM results.

271

272 **Experimental pottery firing at Saran: Testing the Triaxe protocol and re-evaluation of**
273 **previous intensity data**

274 An experimental pottery firing was performed on the 14th of November 2009 at the site
275 of Lac de la Médecinerie (Millet et al., 2015). For this experiment, the well-preserved kiln
276 F196 dated to the 9th century AD was chosen and reconstructed using local clay (Fig. 2a).

277 This kiln is 4 m long and has a wide-open heating chamber, 1.3 m in diameter at the base and
278 1.10 m at the top. Kilns with an open heating chamber were most probably used during the
279 whole period of activity in Saran. Here, the heating was conducted using two fires, one at the
280 entrance of the kiln and the second above the heating chamber (Fig. 2a). Pots were prepared
281 using the clay from a nearby pit, where a potter wheel dated from the 7th century was
282 discovered. Sixty pots were shaped following the known repertoire of forms in Saran for the
283 Early Middle Ages (Fig. 2b). The heating and cooling during the firing was monitored using a
284 single thermocouple placed inside the flue under the vessel chamber (Fig. 2c). From an
285 archeological point of view, this experiment showed that the options chosen for the kiln
286 reconstruction and the firing were appropriate. Indeed, the new ceramics appear very similar
287 to the Saran production of the 7th century. This experiment also provided a rare opportunity to
288 analyze modern ceramics produced in known thermal and magnetic field conditions, and thus
289 to reassess the accuracy of the intensity determinations performed using the Triaxe protocol.
290 For this, direct geomagnetic intensity measurements were carried out inside and outside the
291 reconstructed kiln. A series of 55 measurements using a fluxgate magnetometer was
292 conducted inside the kiln when first full of pottery, then half loaded and finally completely
293 empty, with measurement points located close to the ceramics, kiln walls and under the vessel
294 chamber. All measurements were very homogeneous, yielding a mean intensity value of
295 47.4±0.4μT. Twenty additional measurements were performed from about 10 m to 40 m in
296 the vicinity of the kiln. They yielded a nearly identical mean intensity value (47.9±0.5μT),
297 also very close to the geomagnetic field intensity measured in the French geomagnetic
298 observatory at Chambon la Forêt (47.7μT), about 20 km northeast of Saran. All these direct
299 measurements show that the kiln and its load do not induce a significant magnetic anomaly,
300 and thus the intensity measured inside the kiln correctly reflects the Earth's magnetic field
301 intensity at Saran. Note that a similar conclusion was reached by Morales et al. (2011) from

direct magnetic measurements performed around and inside a small original and open artisanal kiln analyzed in Mexico.

Intensity experiments were conducted on 6 modern pots with two specimens analyzed per pottery (group SAR00). Ten additional pots were tested but the specimens were found to be too weakly magnetized to be analyzed using the Triaxe (i.e. with a moment of less than 40 10^{-8} A.m^2; note that our sampling could not be extended as the pots are to be exhibited). Magnetic susceptibility, IRM acquisition, hysteresis and three-axis IRM measurements were also carried out on this modern material, and the results will be discussed below together with those obtained from the ancient ceramics. The intensity results obtained on the 6 analyzed pottery satisfy our set of quality criteria. As per usual, the intensity results have been first averaged at the specimen level, then at the fragment level, and finally at the group level. This yields a mean intensity value of 46.6±1.2μT (Table 1), which is in good agreement with the direct intensity measurements performed inside and nearby the kiln. This test thus highlights two points: the reliability of the experimental protocol developed for the Triaxe magnetometer and the great potential of the ceramic production at Saran for characterizing the geomagnetic field intensity variations during the Early Middle Ages.

The temperature measurements performed during the experimental firing were also used for assessing the cooling rate effect on TRM acquisition in the case of intensity determinations derived from a more classical method (Genevey and Gallet, 2002). They showed that for this type of rather small kiln with an open heating chamber**,** the cooling was very rapid, with temperatures decreasing from 1000°C to 50°C in less than five hours (Fig. 2c). This observation led us to reconsider the intensity results previously obtained from two groups of ceramics produced at Saran (Genevey and Gallet, 2002). We recall that these data were obtained using the Thellier and Thellier (1959) method as revised by Aitken et al. (e.g. 1988; hereafter referred to as TT-IZ method) and the cooling rate correction was determined

from the comparison of two TRMs acquired from 450°C, one using a rapid cooling rate (as used during the intensity experiments, i.e. ~30 min from 450°C), the second using a slow cooling rate chosen to mimic the original medieval cooling. Genevey and Gallet (2002) used a slow cooling time of 10 hours to decrease the temperature from 450°C to about 25°C. The latter rate was relatively rapid (chosen because the kilns in Saran are small) but not as rapid as that indicated by the experimental firing. Because this difference may lead to an overestimated cooling rate correction, we conducted new experiments (i.e. on new specimens) on the cooling rate effect using a slow cooling time of 4 hours between 450°C and room temperature (Fig. 2c). We have reanalyzed all fragments successfully studied in 2002, plus two fragments, which were rejected because of alteration detected during the cooling rate experiments but not during the intensity measurements (with positive checks for the stability of the partial thermoremanent magnetization, i.e. positive pTRM-checks). We point out that the cooling rate experiments and the intensity measurements were not performed on the same specimens. For the two previously rejected fragments, the new experiments were successful (i.e. no alteration detected), allowing us to consider them now for intensity determination. Overall, these new cooling rate experiments demonstrate that the cooling rate corrections applied in 2002 were overestimated by 1% to 6%. Using the new corrections, we thus revised the two intensity values previously obtained at Saran (supplementary Table S1).

In addition, Triaxe intensity measurements were carried out on four fragments from the same groups. Here we were limited by the relatively weak magnetization of the fragments and by the fact that there was sometimes not enough material for new measurements. Hence only two fragments from group A36 and two from group A38 allowed a direct comparison between Triaxe and TT-IZ intensity results. At the fragment level, three fragments out of four yield similar intensity values to within 2.5% (supplementary Table S1). For fragment A38-06, the Triaxe intensity value appears about 7% higher than the TT-IZ value (79.9μT versus

352 73.8μT), even after the reevaluation of the cooling rate correction. This may be due to
353 differences in the cooling rate experienced by the pottery with respect to their position in the
354 kiln as discussed by Morales et al. (2011). In this case, the duration of 4 hours for the cooling
355 time from 450°C would be too long. Another option would be a bias in the TT-IZ
356 determination that, however, remains unclear. Interestingly, we note that the Triaxe value
357 obtained for this fragment is in good agreement with the other TT-IZ results (supplementary
358 Table S1). Even though the small number of Triaxe results limits the significance of such a
359 comparison, the Triaxe and TT-IZ group-mean intensity values agree to within 3.5% for both
360 A36 and A38. We then combined the Triaxe and TT-IZ results at the fragment level to
361 compute general mean intensity values for these two groups. Group A36 was further
362 complemented by the new Triaxe results obtained from group SAR08, which was collected
363 from exactly the same archeological ensemble. Finally, we underline here that the ages of the
364 A36(/SAR08) and A38 groups were slightly modified by 25 years, with respect to the
365 publication of Genevey and Gallet (2002), in order to take into account the refinement of the
366 chrono-typology since then (Jesset 2013, 2015b; Bouillon, 2015).
367
368 **Magnetic Mineralogy**
369 The aim here is to characterize the magnetic mineralogy of the pottery fragments
370 fulfilling the quality criteria considered for our archeointensity experiments. All these
371 fragments display reversible susceptibility curves after heating to 500°-550°C (Fig. 3). When
372 heating is conducted to 700°C, the χ(T) curves are still reversible, even though a limited
373 alteration is observed in some potsherds (Fig. 3). Most of the χ(T) curves show a single
374 inflection point between 520°C and 570°C, while another inflection point between 200°C and
375 300°C is only observed in a few cases (Fig. 3e).

The saturation of the magnetization is never reached in a field of 1T (Fig. S1a). However, the hysteresis loops are only rarely constricted (Fig. S1b-d). The three-axis IRM experiments clearly show for most fragments the predominance of a magnetic mineral of low coercivity (<0.2T) and unblocking temperatures of less than 550°C, which are typical of magnetite with possible impurities (Fig. 4a,b). We note that the presence of titanium was observed for the Saran production from inductively coupled plasma atomic emission spectroscopy (Bocquet-Liénard and Birée, 2014). The hard components (0.4T and 1.25T) indicate the presence in variable proportions of a mineral of high coercivity, whose unblocking temperatures range between 200°C and 250°C (Fig. 4a-f). We note that this mineral, whose precise identification is still debated (Mcintosh et al., 2007, 2011), is quite frequent in archeological baked clay fragments, whatever their age and their geographic origin (e.g. Chauvin et al., 2000; Genevey and Gallet, 2002; Hartmann et al., 2011). Furthermore, a behavior more typical to that of (titano)hematite is observed for most samples from the thermal demagnetization of the hard component between 550°C and 650°C (Fig. 4d-f). But this magnetic phase is only present in small amounts as it was not detected from the susceptibility measurements (Fig. 3).

Our experiments were complemented by a set of IRM data acquired up to 9T from six fragments. Two of which are representative of the majority of the collection, i.e. with a magnetization predominantly carried by the (titano) magnetite phase (Fig. 4a,b), whereas the four other fragments contain in a relatively large proportion the mineral of high coercivity and low unblocking temperatures previously characterized from the three-axis IRM results (Fig. 4c-f). In all cases, the magnetization saturation is reached at around 3.5T (Fig. 4g). On the other hand, the behavior between ~0.2T and ~3T is entirely controlled by the ratio between the high-coercivity and the (titano) magnetite phases (Fig. 4g). For the weak ratios (SAR08-

19), a first plateau is seen below 0.3T and corresponds to the saturation of the magnetite phase, while for the large ratios (SAR25-05, SAR18-11), no plateau is observed.

Finally, it is worth mentioning that the magnetic mineralogy of the fragments (including those from the modern production) that provided accepted archeointensity data, appears very similar to that encountered in our previous studies (Genevey and Gallet, 2002; Genevey et al., 2009, 2013). The magnetization is hence dominated by (titano) magnetite that conveys the geomagnetic information. It further involves a varying fraction of a magnetic phase characterized by low-unblocking temperatures (200°-250°C) and high coercivity (~3.5T), as well as traces of a more standard hematite demagnetized above ~550°C.

Intensity Results

The success rate of the Triaxe measurements varies among the different fragment groups, ranging from 24% to 89%. All the intensity results obtained at the specimen level (with a total of 276 specimens from 134 independent fragments) are reported in the supplementary Table S2. We note that this success rate is relative to the number of fragments whose magnetization was sufficiently strong to be analyzed using the Triaxe magnetometer. In some cases, this limitation has significantly reduced the number of fragments available for intensity measurements (supplementary Table S2). The intensity results from 7 groups, plus those obtained from the modern pots are displayed in Figure 5 (one panel per group). In this representation, each curve represents the R'(Ti) data obtained for one specimen leading on average to a mean intensity value at the specimen level. For each group, the individual curves appear coherent both at the specimen and fragment levels, which allows us to compute a precise group-mean intensity value with a standard deviation of less than 5% (Table 1).

It is worth pointing out that for the two groups SAR13 and SAR14, associated with two different filling phases inside the same kiln but sharing the same archeological dating, the

425 two mean intensity values are in very good agreement (Table 1). This indicates that the time
426 interval between the two filling phases was most probably short. For this reason, we averaged
427 together all the results from these two groups to obtain a single mean intensity value for the
428 composite group SAR13+SAR14 (Table 1).

429 One of the main causes of rejection in our intensity experiments was related to the
430 overlapping of two components of magnetization making it difficult to reliably isolate a
431 primary magnetization component (Fig. 6a). This observation indicates that some pots broke
432 during the manufacturing process. In fact, this type of incident principally occurs during the
433 early stage of firing because of a very rapid temperature increase inducing stresses in the clay.
434 The presence of two magnetization components in some fragments could therefore indicate
435 reorganization or rebalancing of the load during cooling (the ceramics being somewhat
436 randomly stacked in the kiln – Fig. 2b), with fragments from broken pots moving abruptly or
437 progressively. However, we underline that, for a certain number of fragments, this complexity
438 did not prevent the determination of a reliable archeointensity value (Fig. 5,6b and
439 supplementary Table S2).

440 Several groups of fragments from Saran were also rejected either because the results
441 did not satisfy our quality criteria or because the fragments were too weakly magnetized to
442 achieve measurements using the Triaxe. This has, unfortunately, been the case for two groups
443 associated to the last period of production in Saran (end of the 10^{th} century and beginning of
444 the 11^{th} century). Another group of fragments from the early phase of ceramic production at
445 Saran (middle of the 6^{th} century) was excluded because the original heating (and cooling) was
446 performed in redox conditions; being conducted in air (i.e. in oxidizing conditions), our
447 intensity experiments therefore led to an alteration of the magnetic mineralogy with a clear
448 lightening of the clay paste (a color similar to that of the later production). Four groups dated
449 to the 9^{th} century AD were also discarded because of a non-ideal magnetic behavior during the

intensity determination (i.e. our quality criteria were not fulfilled). The preparation of these particular specimens revealed a soft paste during drilling. As these groups are from the period when the quality of Saran production had declined, it is tempting to relate our failed intensity determinations to this loss of quality. Another possibility, however, would be a relationship with the technical evolution observed from the middle of the 8th century in the morphology of the kilns. This evolution is marked by a kiln floor, which is no longer horizontal but inclined in order to improve the circulation of hot air, which is most probably accompanied by a less open heating chamber (Jesset, 2015a).

Our new archeointensity data for the Early Middle Ages are plotted in Fig. 7. They show that this period was characterized by a rapid intensity increase during the 6th century AD, before a high level of intensity (almost twice that of the present-day field) between the 7th and the 9th century. However, a relative intensity minimum, here documented by two intensity data, likely occurred at the transition between the 7th and the 8th century. Finally a rapid intensity decrease occurred from the middle of the 9th to the beginning of the 11th century, whose averaged variation rate, of the order of ~0.10μT/year, is similar to the one observed during the 6th century. We note that this value is similar to the maximum variation rate observed in the present-day geomagnetic field (Livermore et al., 2014).

Geomagnetic field intensity variations in Western Europe over the past 1500 years

In Western Europe, the variations in geomagnetic field intensity during the Early Middle Ages have long remained poorly documented. Several studies, however, have improved this situation (e.g. Genevey and Gallet, 2002; Donadini et al, 2008, 2012; Gómez-Paccard et al., 2012). This study contributes to this effort with 19 new archeointensity data from the 6th to the 10th century AD, which allows us to decipher the intensity variations over the past 1500 years. Here we discuss that evolution using the archeointensity data obtained in

two circular areas centered on Paris. The first is an area with a 700 km radius around Paris (the geographical area covered by our data), while the second region, with a radius of 1250 km, allows us to significantly increase the dataset with, in particular, the inclusion of numerous results from Spain (e.g. Gómez-Paccard et al., 2006, 2008, 2012; Fig. 1a). For the area of radius 700 km, we have further proceeded in two steps; first considering only our results, which form a homogeneous collection of data, and then all the results available within this area fulfilling a set of selection criteria (see below).

Our data collection comprises 70 intensity results dated from the 5th to the middle of the 19th century (Genevey and Gallet, 2002; Gallet et al., 2005, 2009; Genevey et al., 2009, 2013 and this study), which share many common characteristics. One concerns their age uncertainties, which are always of less than 100 years (this is a selection criterion for our sampling). But, in most cases (i.e. 60 data), the dating precision is less than 50 years. A large majority of the data was obtained using the Triaxe protocol alone or combined with data derived using more classical intensity procedures (in this case, with an agreement within ~5% between the respective means). Only five groups of fragments from this collection were analyzed using solely the TT-IZ (Aitken et al., 1988) or TT-IZZI (Yu et al., 2004) protocols. Finally, the quality criteria used to retain the mean intensity values have remained unchanged throughout our different studies, which further contributes to the homogeneity of this dataset.

The selection of the other archeointensity data also relies on a set of quality criteria (see also Genevey et al., 2009, 2013). These criteria first relate to the intensity method used: the selected data are obtained using either the Thellier and Thellier (1959) method and derived protocols including at least two pTRM-checks or the original Shaw method (1974). The number of results used to compute a mean intensity must be larger or equal to 3 (regardless of the definition of the archeomagnetic site, i.e. fragment or group of fragments) and the error of the corresponding mean value must be of less than 15%. In addition, the TRM

500 anisotropy must be taken into account for artifacts usually considered more sensitive to this
501 effect, such as pottery or tiles (e.g. Genevey et al., 2008). For the dating, we alternatively
502 removed and introduced a criterion on the age uncertainties (i.e. within 100 years) in order to
503 investigate its influence.

504 For the computations of a master curve, we used the least-squares method developed
505 by Thébault and Gallet (2010) that relies on a cubic B-splines time parameterization, with an
506 even time distribution of the spline knots, and on an iteratively reweighting scheme allowing
507 the detection and the weighting of the data appearing as outliers. The method includes a
508 bootstrap approach to account for the experimental and age uncertainties of the data. From the
509 bootstrap resampling technique, the code estimates a large ensemble of individual maximum
510 likelihood curves (about 60000), reconstructs the probability density distribution (pdf) of the
511 maximum likelihood, and then displays its variability at 95% (i.e. the envelope containing
512 95% of the individual curves) and a 95% confidence interval obtained using a classical
513 weighted least-squares inversion. In addition, the self-consistency of the data uncertainties is
514 explored for each model through the computation of the normalized root mean square
515 (NRMS) that evaluates the ratio between the *a posteriori* and *a priori* errors assumed for the
516 data (i.e. the ratio between the distance of the data to the model and the original error attached
517 to the data). It is important to stress that the bootstrap resampling method aims at enhancing
518 only the patterns common to all individual curves estimated after resampling within the dating
519 and experimental data uncertainties. The final master curve is in general smoother, but more
520 robust, than the curve estimated via simple weighted least-squares.

521 The different datasets discussed above are displayed in Figure 7 together with the
522 corresponding master curves. When considering only our collection of data, the derived
523 master curve clearly shows the occurrence of five intensity maxima, at the transition between
524 the 6^{th} and 7^{th} century AD, at the middle of the 9^{th} century, during the 12^{th} century, in the

second part of the 14th century and at the very beginning of the 17th century (Fig. 7a and Table 2; see also Genevey et al., 2013). That computation is characterized by a mean NRMS of 1.10±0.12, which underlines for this dataset the self-consistency between the *a priori* and *a posteriori* data uncertainties. In this case, the 95% fluctuation envelope and the 95% confidence interval match almost perfectly (Fig. 7a). The incorporation of 22 data acquired in the same geographical area (i.e. 700 km around Paris; Fig. 1a) does not markedly change the previous description of the field behavior (Fig. 7b,e and Table 2). However, the mean NRMS for this curve is larger (1.43 ±0.13), which indicates that the model could not fit all data within their *a priori* errors. This is also expressed in Fig. 7b by the fact that the 95% confidence interval becomes wider than the 95% fluctuation envelope of the master curve. Nevertheless, the additional data allow to better document both the significant increase and decrease in geomagnetic field intensity that bound (and characterize) the Early Medieval period, whereas our new data tend to reduce the amplitude of the intensity variations previously suggested by Gómez-Paccard et al. (2012), in particular with a less pronounced relative intensity minimum at the transition between the 7th and the 8th century AD.

Regarding the data reported in Gómez-Paccard et al. (2012), one was obtained in Saran from a series of bricks from kiln F256 excavated at the Zac des Vergers site (laboratory code 45302A; mean intensity at Paris: 80.6±8.3μT). After its abandonment, the kiln was filled with pottery fragments, whose typo-morphology was used to determine its dating. In this study, we analyzed a group of potsherds (A36/SAR08) found in this filling, which gave a mean intensity at Paris of 72.7±3.6μT (Table 1). Although the two intensity results are compatible within their error bars, we cannot exclude the fact that the field intensity during the last use of the kiln was slightly higher than the intensity at the time of production of the pottery found inside the kiln (we further note that Gómez-Paccard et al. (2012) applied a slow cooling time of 24 hours for correcting their data from kiln F256 which, according to the

550 experimental firing described in this study, may lead to an under-estimated mean intensity
551 value). This difference is in agreement with the moderate decrease in intensity observed
552 between the early 7th century and the transition between the 7th and 8th century (Fig. 7a,b). We
553 note, however, that a time lag between the two contexts is not the most likely option from an
554 archeological point of view.

555 Further extending the geographical area of the data to 1250 km (Fig. 1a,7c) does not
556 have any real impact on the reconstruction of the intensity evolution during the Early
557 Medieval period because only three results are added to the previous dataset. By contrast, the
558 number of results dated after the 10th century is significantly increased (Fig. 7e). In particular,
559 the dataset now includes the numerous results obtained in Lübeck (Germany; Schnepp et al.,
560 2009), whose dating was constrained by a time-sequential relationship based on the
561 stratigraphy. It is worth mentioning that this chronology was taken into account for the
562 computation of the probability density function (as was also the case for data obtained by
563 Gómez-Paccard et al., 2006; 2008). As previously discussed in Genevey et al. (2009, 2013),
564 the extended dataset provides a master curve characterized by smooth fluctuations between
565 ~1200 and 1600 AD, which is due to the scatter between the data. Here the degraded internal
566 consistency of the dataset, considered as a whole, is expressed by a NRMS of 1.71±0.13. This
567 dispersion most probably arises from underestimated experimental uncertainties and/or dating
568 errors for some data, as well as from a possible (though likely limited) effect due to secular
569 variation within the rather large geographical area of concern (Casas and Incoronato, 2007).
570 Not surprisingly, introducing a selection criterion of the data based on the dating precision
571 (i.e. within 100 years) decreases the NRMS to 1.63±0.13 and we can better recognize the
572 intensity peaks observed in Fig. 7a,b (Genevey et al., 2013).

573 Detailed comparisons with geomagnetic field intensity variation curves deduced from
574 regional and global archeomagnetic field models were already described in Genevey et al.

575 (2013). The new results reported in this study, focused only on the Early Middle Ages, do not
576 change the main conclusions, in particular regarding the detection from the field models of
577 three intensity maxima observed in Western Europe from the 11th century onwards (Fig. 8a-e,
578 where geomagnetic field models only incorporating volcanic and archeological data were
579 used: Pavón-Carrasco et al., 2009, 2014b; Korte and Constable, 2009; Licht et al., 2013). The
580 regional field modeling constructed by Pavón-Carrasco et al. (2009), that was derived without
581 the archeointensity data obtained by Gómez-Paccard et al. (2012), provides the best evidence
582 for the succession of five intensity maxima since the fifth century AD (Fig. 8a,e). Only the
583 amplitude of the intensity peak at the transition between the 6th and 7th century AD differs
584 significantly. These models were principally constrained by the intensity data obtained in
585 Eastern Europe, mainly in Bulgaria where the dataset was recently updated (Kovacheva et al.,
586 2014). Following Tema and Kondopoulou (2011), we selected the data available within a
587 radius of 700 km around Thessaloniki. Furthermore, as in Genevey et al. (2013), we released
588 the selection criterion relying on the use of pTRM-checks for testing the thermal stability of
589 the magnetic mineralogy of the studied archeological artifacts. Otherwise this would have led
590 to the rejection of a large proportion of this collection of data; it is worth recalling that the
591 same approach applied to the Western European data set would not alter the results shown in
592 Fig. 7. The resulting Balkan master curve given in Figure 8f shows a series of intensity
593 maxima more or less in phase with that from Western Europe, except for the peak around 850
594 AD in Western Europe (Fig. 8a,f). Moreover, the amplitudes of the relative maxima
595 significantly differ between the two European regions. At this stage, we note that searching
596 for evidence of a westward drift in geomagnetic field intensity fluctuations from a comparison
597 between figures 8a and 8f appears inconclusive, or at least premature.
598 Figure 7 strongly supports the idea that the Western European region was characterized by
599 five geomagnetic field intensity maxima over the past 1500 years. What is particularly

striking is the recurrence of these peaks. This can be quantified using a Fourier analysis, which indicates the occurrence of a signal with a pseudo period of ~250 years (Fig. 9). It is worth mentioning that this period is data-driven, based on a coherent dataset, and not introduced by the modeling procedure. We venture that this feature betrays a genuine characteristic of the secular variation, at least in Western Europe, which could be related to a wave motion in the liquid core (e.g. Finlay and Jackson, 2003; Buffett, 2014). In any case, it will require further testing, in particular by continued data acquisition from older periods for which the present scatter observed between the available data prevents a robust analysis (e.g. Gallet et al., 2009; Pavón-Carrasco et al., 2014a).

Conclusions

The results of this study can be organized around five main points:

1. A good agreement is obtained between directly measured geomagnetic field intensities inside or in the periphery of an ancient kiln reconstructed for an experimental firing and the mean intensity value derived from the analysis of pottery produced during this firing. Such agreement confirms and strengthens the reliability of the experimental protocol (and of our selection criteria) developed for the Triaxe magnetometer. This also demonstrates the potential of the ceramic production at Saran to recover the geomagnetic field intensity variations during the Early Middle Ages.

2. Our data show that the magnetic mineralogy of the pottery produced at Saran between the 6th and the 10th century AD is dominated by magnetite, which may have titanium impurities. Another magnetic phase characterized by high coercivity and low unblocking temperatures (200°-250°C) is often present in various proportions. Here we show that this phase is saturated in fields of about 3.5T.

3. We obtain 19 new archeointensity data spanning the Early Middle Ages, a period which was until now very poorly documented in Western Europe. The geomagnetic field intensity variations are characterized by a rapid increase during the 6th century AD, then by high intensity values from the 7th to the 9th centuries and finally by a strong decrease until the beginning of the 11th century. A minimum in intensity of small amplitude is also observed at the transition between the 7th and the 8th century AD.

4. We construct a master curve covering the past 1500 years using a selection of data obtained within 700 km around Paris. This curve clearly exhibits five intensity maxima, at the transition between the 6th and the 7th century AD, at the middle of the 9th century, during the 12th century, in the second part of the 14th century and at the very beginning of the 17th century AD. Some of the peaks are smoothed, or nearly absent when the selection of the data is extended to a radius of 1250 km around Paris.

5. We note that the intensity peaks observed in Western Europe over the past 1500 years occur every ~250 years. This regularity, unnoticed until now, might reflect a new characteristic of the secular variation, at least in Western Europe. It clearly requires further testing, in particular focusing on older periods.

Acknowledgements

We thank the « Fédération Archéologique du Loiret » for their support. We also thank Olivier Labat and the Service Archéologique Départemental des Hauts de Seine, for allowing the sampling from the archeological site, 20 Place de la République, at Vanves. We are grateful to France Lagroix for fruitful discussions on the rock magnetic results, to Fernando Lopes for his help on the spectral analysis and to Ruven Pillay for his very careful reading of the manuscript. We further thank Elisabeth Schnepp and Edvokia Tema who reviewed the paper and made helpful comments. This is IPGP contribution no. 3755.

649

650 **References**

651 Aitken, M. J., Allsop, A. L., Bussell, G. D., Winter, M. B., 1988. Determination of the
652 intensity of the Earth's magnetic field during archaeological times: Reliability of the
653 Thellier technique. Rev. Geophys., 26, 3-12.

654 Aitken, M. J., Allsop, A. L., Bussell, G. D., Liritzis, Y., Winter, M. B., 1989. Geomagnetic
655 intensity measurements using bricks from Greek churches of the first and second
656 millennia A.D.. Archaeometry, 31, 77–87.

657 Bocquet-Liénard, A. and Birée, L., 2014. Caractérisation par ICP-AES des productions des
658 ateliers de Saran (Loiret). In: Bouillon, J., 2015. Loiret, Saran, Ancienne route de
659 Chartres, au lieu-dit « La Guignace » - (zone sud et zone nord). Une extension nord au
660 complexe artisanal potier de Saran « La Médecinerie » (VI^{e}-X^{e} siècle), Rapport de fouille,
661 INRAP Centre Île-de-France.

662 Bouillon, J., 2015. Loiret, Saran, Ancienne route de Chartres, au lieu-dit « La Guignace » -
663 (zone sud et zone nord). Une extension nord au complexe artisanal potier de Saran « La
664 Médecinerie » (VI^{e}-X^{e} siècle), Rapport de fouille, INRAP Centre Île-de-France.

665 Buffett, B., 2014. Geomagnetic fluctuations reveal stable stratification at the top of the
666 Earth's core. Nature, 507, 484–486, doi:10.1038/nature13122.

667 Casas, L., Shaw, J., Gich, M., Share, J. A., 2005. High-quality microwave archaeointensity
668 determinations from an early 18th century AD English brick kiln. Geophys. J. Int., 161,
669 653–661.

670 Casas, L., Incoronato, A., 2007. Distribution analysis of errors due to relocation of
671 geomagnetic data using the 'Conversion via Pole' (CVP) method: implications on

archeomagnetic data. Geophys. J. Int., 169, 448–454. doi:10.1111/j.1365-246X.2007.03346.x.

Catanzariti, G., Gómez-Paccard, M., McIntsosh, G., Pavón-Carrasco, F. J., Chauvin, A., Osete, M. L., 2012. New archaeomagnetic data recovered from the study of Roman and Visigothic remains from central Spain (3rd–7th centuries. Geophys. J. Int., 15pp., doi: 10.1111/j.1365-246X.2011.05315.x.

Catteddu, I., 2009. Archéologie médiévale en France, Le premier Moyen Âge (Ve-XIe siècle). coll. "Archéologie de la France", La Découverte, Paris.

Chapelot, J., 1973. L'atelier céramique carolingien de Saran (Loiret) : les fouilles de 1969 à 1972. Bulletin de la Société Archéologique et Historique de l'Orléanais, nouvelle série, t.VI, 43, 49-72.

Chauvin, A., Garcia, Y., Lanos, P., Laubenheimer, F., 2000. Paleointensity of the geomagnetic field recovered on archaeomagnetic sites from France. Phys. Earth Planet. Inter., 120, 111–136.

Davis, R.H.C., 2005. A History of Medieval Europe: From Constantine to Saint Louis, 3rd Edition, Routledge, 496pp.

Devroey, J.-P., 2003. Economie rurale et société dans l'Europe franque (VI^{e}-IX^{e} siècle), Tome 1, Belin.

Donadini, F., Kovacheva, M., Kostadinova, M., Hedley, I.G., Pesonen, L.J., 2008. Palaeointensity determination on an early medieval kiln from Switzerland and the effect of cooling rate. Phys. Earth. Planet. Inter., 33, 449–457.

Donadini, F., Motschi, A., Rösch, C., Hajdas, I., 2012. Combining an archaeomagnetic and radiocarbon study: dating of medieval replaces at the Mühlegasse, Zürich. J. Archaeol. Sci., 39, 2153–2166.

696 Evans, M. E., 1986. Paleointensity estimates from Italian kilns. J. Geomagn. Geoelect., 38,
697 1259–1267.

698 Finlay, C. C., Jackson A., 2003. Equatorially dominated magnetic field change at the surface
699 of the Eath's core, Science, 300, 2084-2086.

700 Gallet, Y., Genevey, A., Fluteau, F., 2005. Does Earth's magnetic field secular variation
701 control centennial climate change?, Earth Planet. Sci. Lett., 236, 339–347.

702 Gallet, Y., Le Goff, M., 2006. High-temperature archeointensity measurements from
703 Mesopotamia. Earth Planet. Sci. Lett., 241, 159–173.

704 Gallet, Y., Genevey, A., Le Goff, M., Warmé, N., Gran-Aymerich, J., Lefèvre, A., 2009. On
705 the use of archeology in geomagnetism, and vice-versa: Recent developments in
706 archeomagnetism. C. R. Physique, 10, 630–648.

707 Games, K. P., Baker, M. E., 1981. Determination of geomagnetic archaeomagnitudes from
708 clay pipes. Nature, 289, 478–479.

709 Genevey, A., Gallet, Y., 2002. Intensity of the geomagnetic field in Western Europe over the
710 past 2000 years: New data from ancient French pottery. J. Geophys. Res., 107, (B11),
711 doi:10.1029/2001JB000701.

712 Genevey, A., Gallet, Y., Constable, C. G., Korte, M., Hulot, G., 2008. ArcheoInt: An
713 upgraded compilation of geomagnetic field intensity data for the past ten millennia and
714 its application to the recovery of the past dipole moment. Geochem. Geophys. Geosyst.,
715 9, Q04038, doi:10.1029/ 2007GC001881.

716 Genevey, A., Gallet, Y., Rosen, J., Le Goff, M., 2009. Evidence for rapid geomagnetic field
717 intensity variations in Western Europe over the past 800 years from new French
718 archeointensity data. Earth Planet. Sci. Lett., 284, 132-143.

719 Genevey, A., Gallet, Y., Thébault, E., Jesset, S., Le Goff, M., 2013. Geomagnetic field
720 intensity variations in Western Europe over the past 1100 years. Geochem. Geophys.
721 Geosyst, Geosystems 14: doi: 10.1002/ggge.20165.

722 Gómez-Paccard, M., Chauvin, A., Lanos, P., Thiriot, J., Jiménez-Castillo, P., 2006.
723 Archeomagnetic study of seven contemporaneous kilns from Murcia (Spain). Phys. Earth
724 Planet. Inter., 157, 16–32.

725 Gómez-Paccard, M., Chauvin, A., Lanos, P., Thiriot, J., 2008. New archeointensity data from
726 Spain and the geomagnetic dipole moment in western Europe over the past 2000 years. J.
727 Geophys. Res., 113, B09103, doi:10.1029/2008JB005582.

728 Gómez-Paccard, M., Chauvin, A., Lanos, P., Dufresne, P., Kovacheva, M., Hill, M. J.,
729 Beamud, E., Blain, S., Bouvier, A., Guibert, P., and Archaeological Working Team,
730 2012. Improving our knowledge of rapid geomagnetic field intensity changes observed in
731 Europe between 200 and 1400 AD. Earth Planet. Sci. Lett., 355–356, 131–143.

732 Gram-Jensen, M., Abrahamsen, N., Chauvin, A., 2000. Archaeomagnetic intensity in
733 Denmark. Phys. Chem. Earth, 25, 525–531.

734 Hartmann, G.A., Genevey, A., Gallet, Y., Trindade, R. I. F., Etchevarne, C., Le Goff, M.,
735 Afonso, M.C., 2010. Archeointensity in Northeast Brazil over the past five centuries.
736 Earth Planet. Sci. Lett., 296, 340–352.

737 Hartmann, G. A., Genevey, A., Gallet, Y., Trindade, R. I. F., Le Goff, M., Najjar, R.,
738 Etchevarne, C., Afonso, M. C., 2011. New historical archeointensity data from Brazil:
739 Evidence for a large regional non-dipole field contribution over the past few centuries.
740 Earth Planet. Sci. Lett., 306, 66-76.

741 Jesset, S., Alenet de Ribemont, G., Dauphin, J., Frenee, E., Georges, P., Josset, D., Le
742 Boulanger, F., Leroyer, C., Lusson, D., Moret-Auger, F., Raux, S., Tribes, L., 2001.

743 Saran (Loiret), «ZAC des Vergers ». Document de fouille de sauvetage, Orléans, SRA
744 Centre, 267pp.

745 Jesset, S., Bouillon, J., Genevey, A., Millet, S., and Warmé, N., 2010. SARAN «Lac de la
746 Médecinerie» (Loiret) 45.302.01-AH. Rapport intermédiaire de fouille programmée,
747 104pp.

748 Jesset, S., 2013. Saran et Orléans: chrono-typologie de la céramique du haut Moyen Âge de
749 l'Orléanais. In: Husi, P. (Ed.), La céramique du haut Moyen Âge dans le Centre-Ouest de
750 la France: de la chrono-typologie aux aires culturelles, La Revue Archéologique du
751 Centre de la France, Supplément 49, 268 pp.

752 Jesset, S., 2015a. Les ateliers de potiers du haut Moyen Âge autour d'Orléans (Loiret) :
753 Caractérisation, organisation et production. In: Thuillier, F., Louis, E., (Ed.), Tourner
754 autour du pot..., Les ateliers de potiers médiévaux du Ve au XIIe siècle dans l'espace
755 européen, Caen, publications du CRAHAM.

756 Jesset, S., 2015b. Les ateliers de potiers de Saran (VI^{e}-X^{e} siècle) : inventaire des productions
757 et de leur diffusion en région Centre, Bulletin annuel de la Société Archéologique et
758 Historique de Beaugency, 40, 3–7.

759 Kondopoulou, D., Zananiri, I., Rathossi, C., De Marco, E., Spatharas, V., Hasaki, E., 2014.
760 An Archaeometric and Archaeological Approach to Hellenistic–Early Roman Ceramic
761 Workshops in Greece: Contribution to Dating. Radiocarbon, 56, S27–S38, doi:
762 http://dx.doi.org/10.2458/azu_rc.56.18340.

763 Korte, M., Donadini, F., Constable, C. G., 2009. Geomagnetic field for 0–3 ka: 2. A new
764 series of time-varying global models. Geochem. Geophys. Geosyst., 10, Q06008,
765 doi:10.1029/2008GC002297.

766 Kovacheva, M., Kostadinova-Avramova, M., Jordanova, N., Lanos, Ph., Boyadzhiev, Y.,
767 2014. Extended and revised archaeomagnetic database and secular variation curves from
768 Bulgaria for the last eight millennia. Phys. Earth Planet. Inter., 236, 79–94

769 Le Goff, M., Gallet, Y., 2004. A new three-axis vibrating sample magnetometer for
770 continuous high-temperature magnetization measurements: Applications to paleo- and
771 archeo-intensity determinations. Earth Planet. Sci. Lett., 229, 31–43.

772 Lefèvre, A., 2007. Vanves (Hauts-de-Seine, France): La découverte d'un important centre
773 potier du Haut Moyen Age. in: 4th International Congress of Medieval and Modern
774 Archeology, 3–8 Sept., 2007, Paris.

775 Lefèvre, A., 2009. Première attestation d'une activité potière médiévale à Vanves (92),
776 l'ensemble de la Place de la République (VIe s.). In: Gentili, F., Lefèvre, A. (Ed.),
777 L'habitat rural du haut Moyen Âge en Île-de-France: 2, Guiry-en-Vexin: Centre de
778 Recherches Archéologiques du Vexin Français.

779 Lefèvre, A., Peixoto, X., 2015. Les ateliers de potiers de la rue Gaudray à Vanves (Hauts-de-
780 Seine) », In: Thuillier, F., Louis, E., (Ed.), Tourner autour du pot..., Les ateliers de potiers
781 médiévaux du Ve au XIIe siècle dans l'espace européen, Caen, publications du
782 CRAHAM.

783 Licht, A., Hulot, G., Gallet, Y., Thébault, E., 2013. Ensembles of low degree archeomagnetic
784 field models for the past three millennia. Phys. Earth. Planet. Inter., 224, 38–67.

785 Livermore, P. W., Fournier, A., Gallet, Y., 2014. Core-flow constraints on extreme
786 archeomagnetic intensity changes. Earth Planet. Sci. Lett., 387, 145–156,
787 doi:10.1016/j.epsl.2013.11.020.

788 Lowrie, W., 1990. Identification of ferromagnetic minerals in a rock by coercivity and
789 unblocking temperatures properties. Geophys. Res. Lett., 17, 159–162. doi:10.1029/
790 GL017i002p00159.

791 McIntosh, G., Kovacheva, M., Catanzariti, G., Osete, M. L., Casas, L., 2007. Widespread
792 occurence of a novel high coercivity, thermally stable, low unblocking temperature
793 magnetic phase in heated archeological material. Geophys. Res. Lett., 34, L21302.
794 doi:10.1029/2007GL031168.

795 McIntosh, G., Kovacheva, M., Catanzariti, G., Donadini, F., Lopez, M. L. O., 2011. High
796 coercivity remanence in baked clay materials used in archeomagnetism. Geochem.
797 Geophys. Geosyst., 12, Q02003, doi:10.1029/2010GC003310.

798 Millet, S., Jesset, S., Bouillon, J., 2015. L'apport des expérimentations et des analyses
799 connexes : l'exemple de Saran 2000 / 2009 (Loiret). In: Thuillier, F. and E. Louis (Ed),
800 Tourner autour du pot… Les ateliers de potiers médiévaux du Ve au XIIe siècle dans
801 l'espace européen, Actes du colloque international de Douai (5-8 octobre 2010),
802 collection Publications du Craham, Presses universitaires de Caen.

803 Morales J., Goguitchaichvili, A., Aguilar-Reyes, B., Pineda-Duran, M., Camps, P., Carvallo,
804 C., Calvo-Rathert, M., 2011. Are ceramics and bricks reliable absolute geomagnetic
805 intensity carriers?. Phys. Earth Planet. Int., 187, 310-321.

806 Pavón-Carrasco, F. J., Osete, M. L., Torta, J. M., Gaya-Piqué, L. R., 2009. A regional
807 archeomagnetic model for Europe for the last 3000 years, SCHA.DIF.3K: Applications to
808 archeomagnetic dating. Geochem. Geophys. Geosyst., 10, Q03013,
809 doi:10.1029/2008GC002244.

810 Pavón-Carrasco, F. J., Gómez-Paccard, M., Hervé, G., Osete López, M. L., Chauvin, A.,
811 2014a. Intensity of the geomagnetic field in Europe for the last 3 ka: Influence of data

812 quality on geomagnetic field modeling. Geochem. Geophys. Geosyst., 15, 2515-2530,
813 doi:10.1002/2014GC00531.

814 Pavón-Carrasco, F. J., Osete López, M. L., Torta, J. M., De Santis, A., 2014b. A geomagnetic
815 field model for the Holocene based on archaeomagnetic and lava flow data. Earth Planet.
816 Sci. Lett., 388, 98–109.

817 Schnepp, E., Lanos, P., Chauvin, A., 2009. Geomagnetic paleointensity between 1300 and
818 1750 A.D. derived from a bread oven floor sequence in Lübeck, Germany. Geochem.
819 Geophys. Geosyst., 10, Q08003, doi:10.1029/2009GC002470.

820 Shaw, J., 1974. A new method of determining the magnitude of the palaeomagnetic field:
821 Application to five historic lavas and five archaeological samples. Geophys. J. R. Astron.
822 Soc., 39, 133–141.

823 Spassov, S., Hus, J., Geeraerts, R., Haller, F., 2008. Archaeomagnetic dating of a High
824 Middle Age likely iron working site in Corroy-le-Grand (Belgium). Phys. Chem. Earth.,
825 33, 544–556.

826 Spassov, S., Valet, J.-P. , Kondopoulou, D., Zananiri, I., Casas, L., Le Goff, M., 2010. Rock
827 magnetic property and paleointensity determination on historical Santorini lava flows.
828 Geochem. Geophys. Geosyst., 11, Q07006, doi:10.1029/2009GC003006.

829 Spatharas, V., Kondopoulou, D., Aidona, E., Efthimiadis, K. G., 2010. New magnetic
830 mineralogy and archaeointensity results from Greek kilns and baked clays. Stu. Geophys.
831 Geod., 55, 131–157.

832 Tema, E., Goguitchaichvili, A., Camps, P., 2009. Archaeointensity determinations from Italy:
833 new data and the Earth's magnetic field strength variation over the past three millennia.
834 Geophys. J. Int., doi: 10.1111/j.1365-246X.2009.04455.x

835 Tema, E., Kondopoulou, D., 2011. Secular variation of the Earth's magnetic field in the
836 Balkan region during the last eight millennia based on archaeomagnetic data. Geophys. J.
837 Int., 186, 603–614, doi: 10.1111/j.1365-246X.2011.05088.x.

838 Tema, E., Morales, J., Goguitchaichvili, A., Camps, P., 2013. New archaeointensity data from
839 Italy and geomagnetic field intensity variation in the Italian Peninsula. Geophys. J. Int.
840 (2013) 193, 603–614, doi: 10.1093/gji/ggs120.

841 Thébault, E., Gallet, Y., 2010. A bootstrap algorithm for deriving the archeomagnetic field
842 intensity variation curve in the Middle East over the past 4 millennia BC. Geophys. Res.
843 Lett., 37, L22303, doi:10.1029/2010GL044788.

844 Thellier, E., Thellier, O., 1959. Sur l'intensité du champ magnétique terrestre dans le passé
845 historique et géologique. Ann. Geophys., 15, 285–376.

846 Thellier, E., 1981. Sur la direction du champ magnétique terrestre en France durant les deux
847 derniers millénaires. Phys. Earth Planet., Int., 24, 89-132.

848 Warmé, N., 2009. L'archéomagnétisme appliqué aux fours culinaires du haut Moyen Âge: 10
849 ans d'activité en collaboration avec le PCR "Habitat rural du haut Moyen Âge". In:
850 Gentili, F., Lefèvre, A. (Ed.), L'habitat rural du haut Moyen Âge en Île-de-France: 2,
851 Guiry-en-Vexin: Centre de Recherches Archéologiques du Vexin Français.

852 Yu, Y., Tauxe, L., Genevey, A., 2004. Toward an optimal geomagnetic field intensity
853 determination technique. Geochem. Geophys. Geosyst., 5, Q02H07.
854 doi:10.1029/2003GC000630.

855

856 **Figure captions**

857 Figure 1: (a) Location map of the three medieval archeological sites of Saran, Ingré and
858 Vanves sampled in this study (pink circles). The blue circles indicate the locations of our data

859 previously obtained in France and for one result from Belgium (Genevey and Gallet, 2002;
860 Genevey et al., 2009, 2013; Gallet et al., 2009). The green squares correspond to published
861 intensity results available within a radius of 700 km and 1250 km around Paris (indicated by a
862 red star). See text in section Geomagnetic field intensity variations in Western Europe over
863 the past 1500 years, for a description of these selected data, which were obtained in Belgium,
864 Denmark, England, France, Germany, Italy, Spain and Switzerland. (b) Photo illustrating a
865 group of pottery fragments, as analyzed in this study. Here the SAR04 group collected at Lac
866 de la Médecinerie in Saran associated to kiln F196. (c) Photo of pots discovered in the filling
867 units of the kiln 1098 during excavations conducted in the street Rue Gaudray in Vanves. The
868 VAN07 group is associated to this kiln © Laurent Petit, Inrap.
869
870 Figure 2: Experimental firing at Saran-Lac de la Médecinerie (a) Kiln F196 after its
871 reconstruction and at the end of the firing. The ashes above the heating chamber attest to the
872 use of a second fire during the heating, in addition to the one located at the kiln entrance (b)
873 Load of the kiln (after baking) - a magnetic probe was inserted inside the kiln in order to
874 directly measure the geomagnetic field intensity (c) Evolution of the temperatures measured
875 by a thermocouple located inside the flue (Millet et al., 2015). The moderate firing during the
876 two first hours was used to dry the clay and avoid cracking in the ceramics. A short episode of
877 rain during the first hour of the cooling may have accelerated the beginning of the cooling,
878 but most likely it did not influence its end. The grey square shows the temperature interval
879 involved in our experiments on cooling rate effect on TRM acquisition. A 4-hour cooling time
880 from 450°C to 30°C was therefore used to mimic the original cooling of the pottery.
881
882 Figure 3: Representative examples of magnetic susceptibility versus temperature curves
883 obtained for fragments fulfilling the quality criteria used for intensity determinations. (a-e)

884 Medieval pottery fragments; (f) Pottery produced during the experimental firing. The heating
885 was first performed up to 500°C-550°C (blue axis in the insets; red/heating and blue/cooling
886 curves). Another heating up to ~680°C was next conducted on new powders (black axis;
887 black/heating and grey/cooling curves).
888
889 Figure 4: Thermal demagnetization of three-axis IRM components acquired in orthogonal
890 fields of 1.25, 0.4 and 0.2T for (a,c,d,e,f) five medieval pottery fragments and (b) a modern
891 ceramic produced during the experimental firing. (g) IRM curves obtained up to 9T acquired
892 on twin specimens for the same 6 fragments as in (a-f).
893
894 Figure 5: Archeointensity results obtained from 7 groups of medieval pottery fragments (one
895 group per archeological site) and from the modern pottery production; one panel for each
896 group of results. Each curve represents the intensity data obtained for one specimen over the
897 temperature interval used for intensity determination.
898
899 Figure 6: (a) Example of a rejected fragment for which the thermal demagnetization during
900 the Triaxe experiment did not allow us to isolate a well-defined primary magnetization
901 component (left panel) and the corresponding R'(Ti) data (right panel). (b) Example of a
902 retained fragment with two magnetization components well isolated during heating, and the
903 corresponding R'(Ti) data before (blue curve, right panel) and after (purple curve, right panel)
904 adjusting the T1 temperature (see text in Section Intensity and Rock Magnetic Experiments).
905 Open (closed) symbols refer to the inclinations (declinations) in the orthogonal vector
906 diagrams. Note that the Triaxe protocol provides measurements every 5°C and that only a
907 subset of the data (every 25°C from 100°C up to the highest temperature) was reported in
908 these diagrams.

Figure 7: Geomagnetic field intensity variations in Western Europe over the past 1500 years. These variations were established from four different datasets: (a) Our data; (b) selected data available within a 700 km radius around Paris (c) within a 1250 km radius around Paris, (d) Same as in (c) but only the data with age uncertainties of less than 100 years are retained. All data were reduced at the latitude of Paris (48.9°N). (e) Age distribution of the first three datasets (respectively in dark blue, light blue and grey). Following Genevey et al. (2008, 2009, 2013), an arbitrary 5% decrease was implemented for the data, indicated by *, for which the cooling rate effect was not originally evaluated. We note that this only concerns 9 data. The master curves are computed using cubic-B splines with 50 years knot spacing and displayed in the form of a probability distribution function (the grey scale in (a) is identical in the other 3 figures). The curves in pink show the maximum likelihood vs. time (solid line) and its variability at 95% (dotted lines). The thin blue dotted lines indicate the 95% confidence interval obtained using a classical least-squares inversion.

Figure 8: Comparison over the past 1500 years of (a) the master curve of the geomagnetic field intensity variations derived from data selected within 700 km around Paris (same as in Fig. 7b) with predictions at Paris from global (b, c, d) and regional (e) archeomagnetic field models computed from the inversion of archeomagnetic and volcanic data only. (b) ARCH3k.1: Korte and Constable (2009); (c) AF_M: Licht et al. (2013); (d) SHA.DIF.14k: Pavón-Carrasco et al. (2014b); (e): SCHA.DIF.3k: Pavón-Carrasco et al. (2009). (f): Selected data obtained within 700 km around Thessaloniki and master curve derived from this dataset (same conventions as in Fig. 7; all data were reduced to the latitude of Thessaloniki, 40.65°N). The data are mainly (~85%) from Bulgaria (Kovacheva et al., 2014) but also from Greece and Southern Italy (Evans, 1986; Aitken et al., 1988, 1989; Tema et al., 2009; Spassov

et al., 2010; Spatharas et al., 2011; Kondopoulou et al., 2014). The NRMS of 2.40±1.60 indicates that the model could not fit a significant number of data with their *a priori* errors.

Figure 9: Spectral analysis of the master curve derived from our dataset. (a) red and blue curves (left axis): Maximum likelihood of the pdf and its trend estimated using a Singular Spectral Analysis; purple curve (right axis) : Residual signal between the master curve and the trend. (b) Power Spectrum Density of the residual signal using Fourier analysis. The observed peak indicates a pseudo periodicity of ~250 years for the intensity maxima.

Table captions:

Table 1: New archeointensity data obtained from the analysis of 20 groups of pottery fragments dated to the Early Middle Ages.

The pottery fragments were produced in Saran (47.9°N, 1.9°N), Ingré (47.9°N, 1.8°E) and Vanves (48.8°N, 2.3°E). SU stands for stratigraphic unit. N frag. (or n spec.), number of different fragments (or specimens) retained for each group for computing a mean intensity value; F±σF, mean intensity at the group-level and its standard deviation in μT; F_{Paris}, mean intensity in μT after reduction to the latitude of Paris (48.9°N) using the hypothesis of a geocentric axial dipole field.

Table 2: Maximum likelihoods of the Western European geomagnetic field intensity variation estimated at Paris from 400 to 1850 AD years and their 95% fluctuation intervals computed in steps of 25 years.

These computations rely firstly on our data and secondly on data available within 700 km around Paris fulfilling selection criteria (see text). They were carried out using the iteratively

958 re-weighted least squares method combined with a bootstrap algorithm developed by
959 Thébault and Gallet (2010).
960
961 **Supplementary material:**
962 Figure S1: (a) Curves of progressive IRM acquisition up to 1T for two fragments from each
963 group. The colored lines (as opposed to the black curves) indicate the fragments (one per
964 group) chosen for the three-axis IRM experiments. The six colored thick curves underline the
965 fragments for which IRM experiments were conducted up to 9T (see Fig. 4g). (b, c) Examples
966 of hysteresis curves, showing non-constriction, usually observed for this collection. (d)
967 Example of hysteresis curve with a wasp-waisted shape.
968
969 Table S1: Revised intensity results obtained for groups A36 and A38 using the Thellier and
970 Thellier method as revised by Aitken et al. (e.g. 1988; TT-IZ) and their comparison with
971 Triaxe intensity determinations.
972 The results were originally published in Genevey and Gallet (2002). A slow cooling time of
973 10 hours from 450°C to room temperature was used at the time for the cooling rate
974 experiments. However, the experimental firing performed in Saran indicated that the original
975 cooling rate was likely faster, requiring a correction to the 2002 intensity data. New cooling
976 rate experiments were performed with a slow cooling time of 4 hours from 450°C to room
977 temperature (see Fig. 2c). The new cooling rate correction factors and the new corresponding
978 intensity results are reported. For each TT-IZ intensity determination at the specimen level: n
979 gives the number of temperature steps, T_{min}-T_{max} indicates the corresponding temperature
980 range, f is for the NRM fraction involved in the computation. Columns g and q display the
981 gap and quality factor as defined by Coe et al. (1978). F_{lab} indicates the intensity of the
982 laboratory field in μT, $H_{non\text{-}corrected}$ the archeointensity before TRM anisotropy and cooling rate

corrections in μT, σF, the standard error in μT, $F_{anisotropy\ corrected}$ the archeointensity after TRM anisotropy correction in μT. $F_{mean\ value\ per\ potsherd\ corrected\ for\ the\ cooling\ rate\ effect}$ and $F_{Triaxe\ mean\ value\ per\ potsherd}$ (see also in Table S2) are given in μT. The F_{mean}±σF (TT-IZ) (resp. Triaxe) column reports the mean intensity at the site level and its standard deviation in μT using the TT-IZ (resp. Triaxe) protocol. The two fragments marked with a star were initially rejected because an alteration occurred during the cooling rate experiments (and not during the TT-IZ experiments with positive pTRM-checks). In these two cases, the new cooling rate experiments were successful, allowing us to retain the fragments. Intensity results are given at the site of Saran (47.9°N, 1.9°N). ** indicates that the dating of the groups were slightly modified by 25 years, with respect to the publication of Genevey and Gallet 2002, in order to integrate new archeological constraints.

Reference:

Coe, R. S., Gromme S., Mankinen E. A., 1978. Geomagnetic paleointensities from radiocarbon-dated lava flows on Hawaii and the question of the Pacific nondipole low, J. Geophys. Res., 83, 1740–1756.

Table S2: Triaxe intensity results obtained at the specimen and fragment levels.

T_{min}-T_{max} indicates the temperature range used for the intensity determinations. H_{lab} is the intensity of the laboratory field in μT. NRM T1 (T1') indicates the % of NRM involved. Slope R' is the slope expressed in % of the line between the first and the last point used for the intensity computations. F_{Triaxe} indicates the intensity value obtained at the specimen level. $F_{Triaxe\ mean\ value\ per\ fragment}$ ±σF indicates the intensity value at the fragment level with its standard deviation. (n1/n2/n3)* indicates for each group the number of collected fragments (n1), the number of fragments whose magnetization was strong enough to be measured using the Triaxe (n2) and the number of fragments which fulfilled our quality criteria (n3).

1008

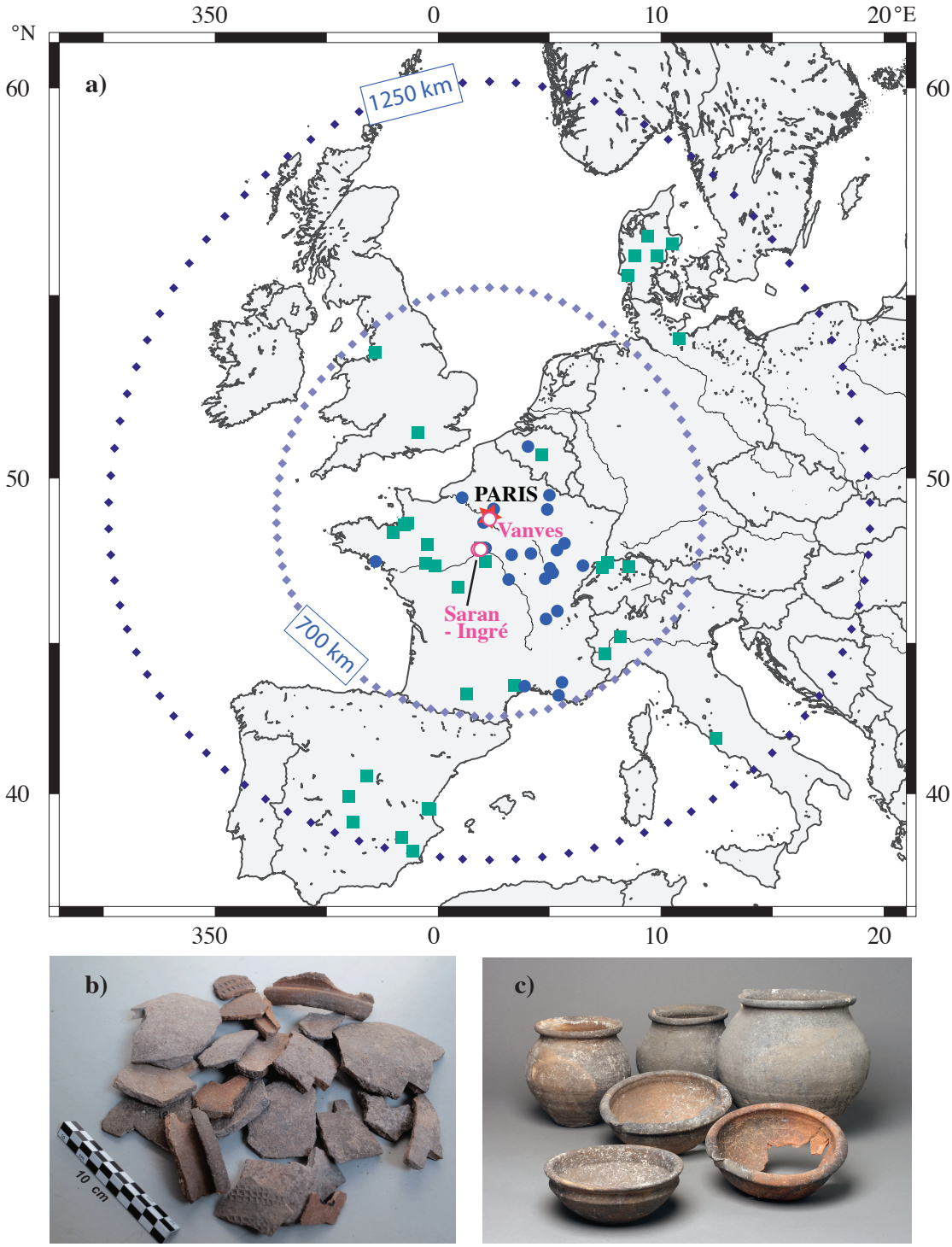
°N
350
0
10
20 °E
60
50
40
a)
1250 km
700 km
PARIS
Vanves
Saran
- Ingré
b)
10 cm
c)

Figure 1

(a)

(b)

(c)

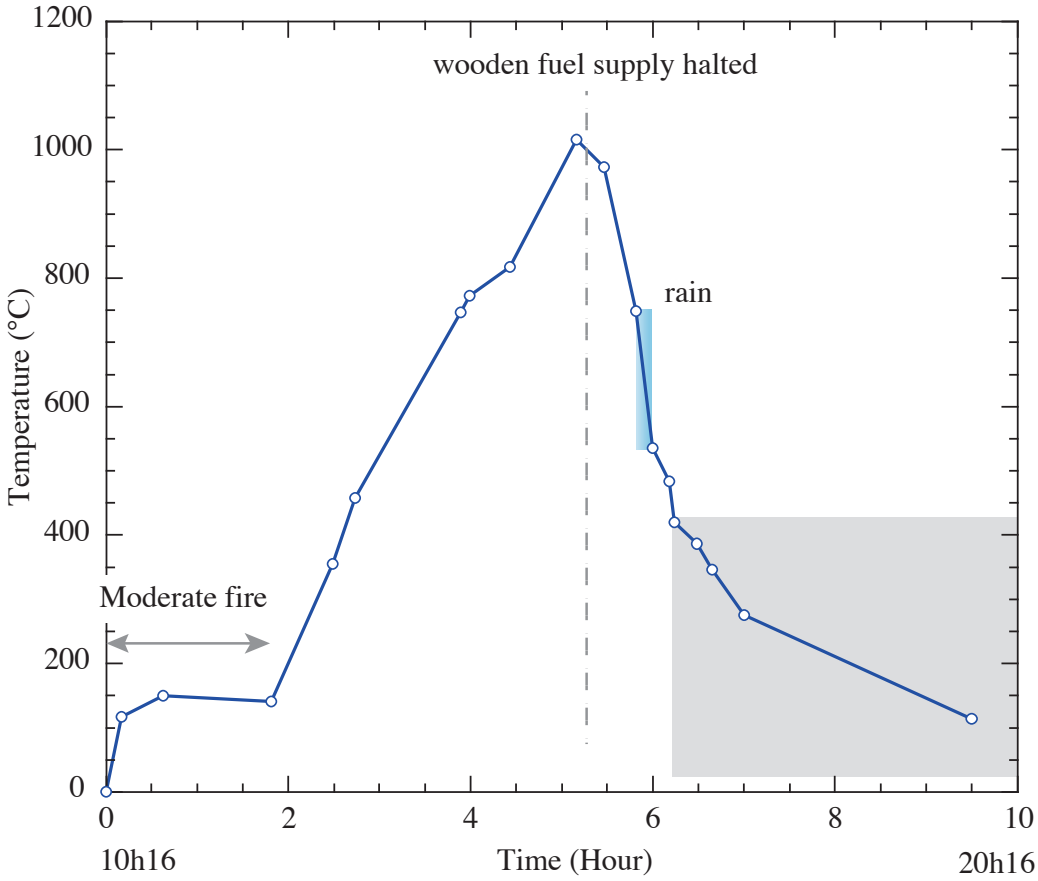
1200
1000
800
600
400
200
0
Temperature (°C)
wooden fuel supply halted
rain
Moderate fire
0
2
4
6
8
10
10h16
Time (Hour)
20h16

Figure 2

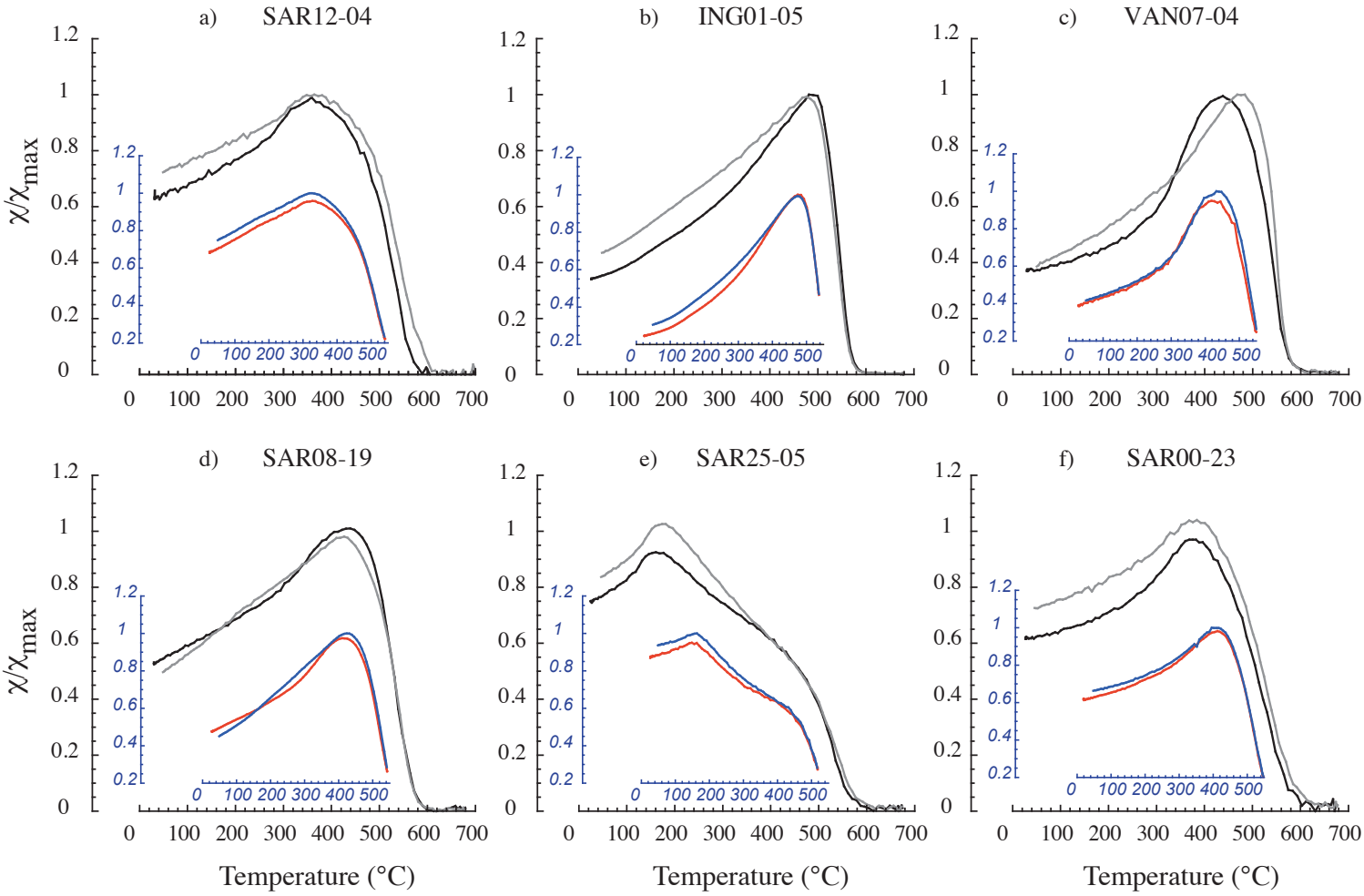
a) SAR12-04
b) ING01-05
c) VAN07-04
d) SAR08-19
e) SAR25-05
f) SAR00-23
χ/χmax
Temperature (°C)

Figure 3

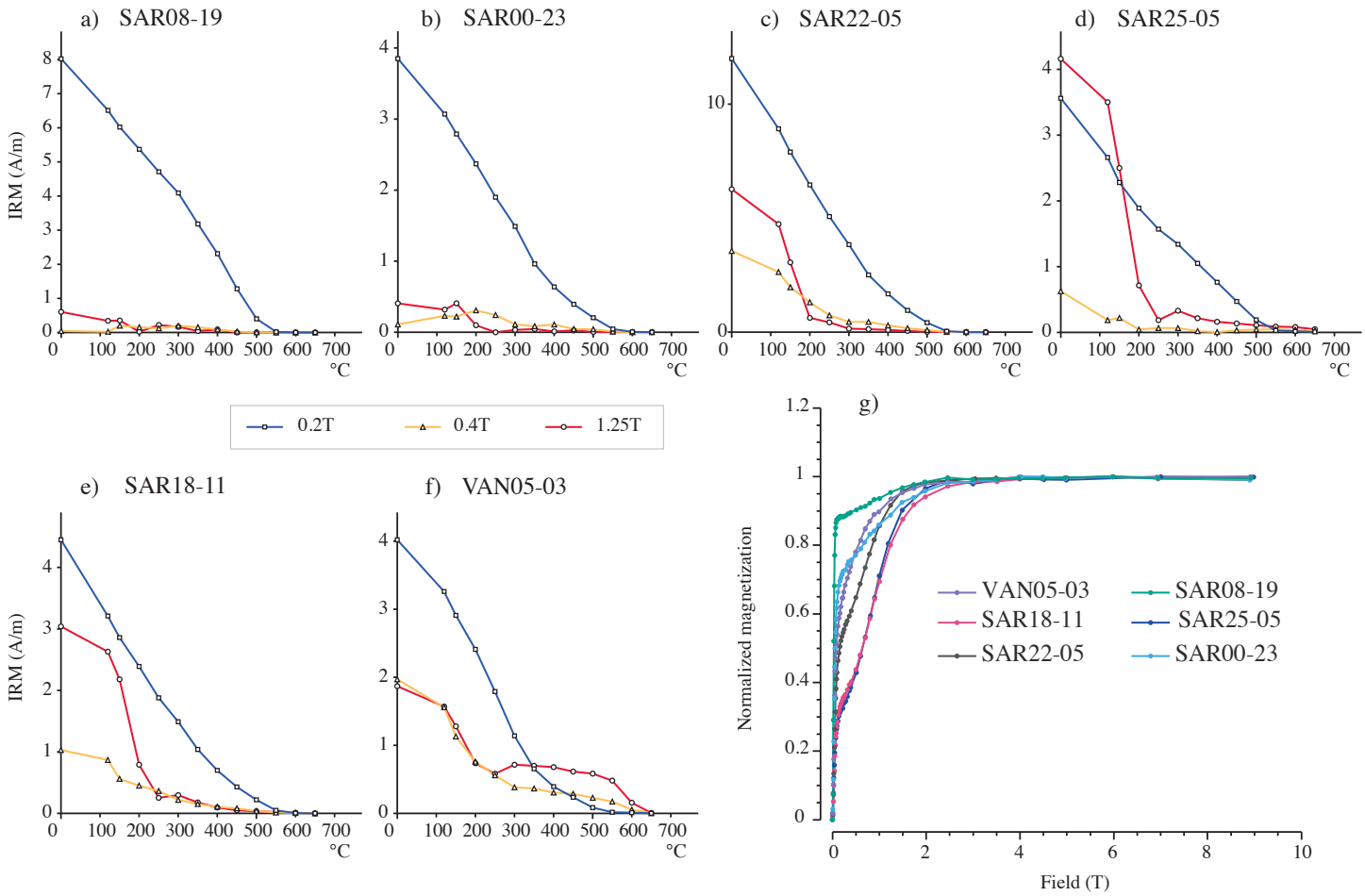
a) SAR08-19
b) SAR00-23
c) SAR22-05
d) SAR25-05
IRM (A/m)
°C
0.2T
0.4T
1.25T
e) SAR18-11
f) VAN05-03
g)
Normalized magnetization
Field (T)
VAN05-03
SAR08-19
SAR18-11
SAR25-05
SAR22-05
SAR00-23

Figure 4

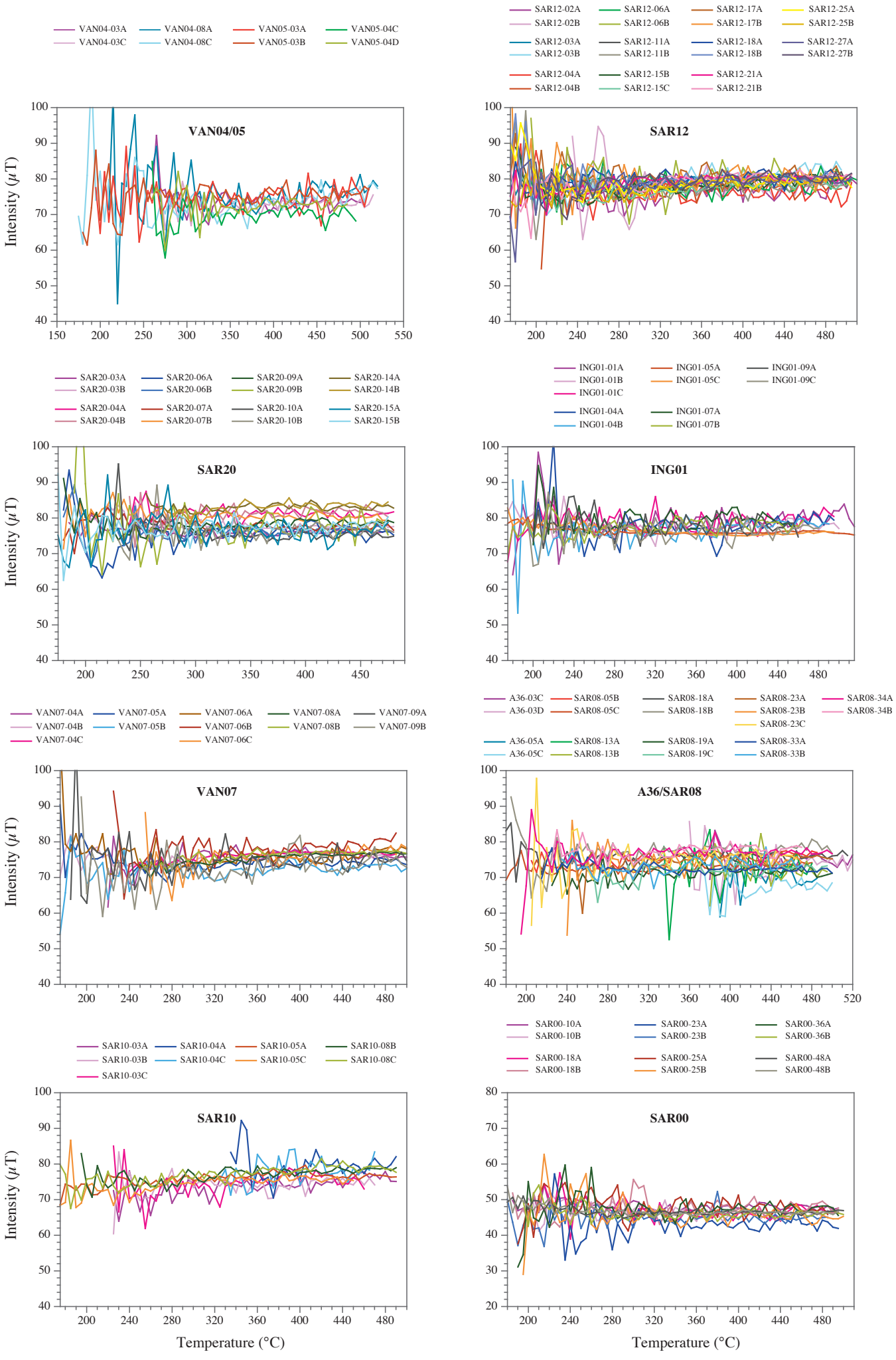
VAN04-03A
VAN04-03C
VAN04-08A
VAN04-08C
VAN05-03A
VAN05-03B
VAN05-04C
VAN05-04D
VAN04/05
Intensity (μT)
SAR12-02A
SAR12-02B
SAR12-06A
SAR12-06B
SAR12-17A
SAR12-17B
SAR12-25A
SAR12-25B
SAR12-03A
SAR12-03B
SAR12-11A
SAR12-11B
SAR12-18A
SAR12-18B
SAR12-27A
SAR12-27B
SAR12-04A
SAR12-04B
SAR12-15B
SAR12-15C
SAR12-21A
SAR12-21B
SAR12
SAR20-03A
SAR20-03B
SAR20-06A
SAR20-06B
SAR20-09A
SAR20-09B
SAR20-14A
SAR20-14B
SAR20-04A
SAR20-04B
SAR20-07A
SAR20-07B
SAR20-10A
SAR20-10B
SAR20-15A
SAR20-15B
SAR20
ING01-01A
ING01-01B
ING01-01C
ING01-05A
ING01-05C
ING01-09A
ING01-09C
ING01-04A
ING01-04B
ING01-07A
ING01-07B
ING01
VAN07-04A
VAN07-04B
VAN07-04C
VAN07-05A
VAN07-05B
VAN07-06A
VAN07-06B
VAN07-06C
VAN07-08A
VAN07-08B
VAN07-09A
VAN07-09B
VAN07
A36-03C
A36-03D
A36-05A
A36-05C
SAR08-05B
SAR08-05C
SAR08-13A
SAR08-13B
SAR08-18A
SAR08-18B
SAR08-19A
SAR08-19C
SAR08-23A
SAR08-23B
SAR08-23C
SAR08-33A
SAR08-33B
SAR08-34A
SAR08-34B
A36/SAR08
SAR10-03A
SAR10-03B
SAR10-03C
SAR10-04A
SAR10-04C
SAR10-05A
SAR10-05C
SAR10-08B
SAR10-08C
SAR10
SAR00-10A
SAR00-10B
SAR00-18A
SAR00-18B
SAR00-23A
SAR00-23B
SAR00-25A
SAR00-25B
SAR00-36A
SAR00-36B
SAR00-48A
SAR00-48B
SAR00
Temperature (°C)
Temperature (°C)

Figure 5

a) SAR07-18

Rejected

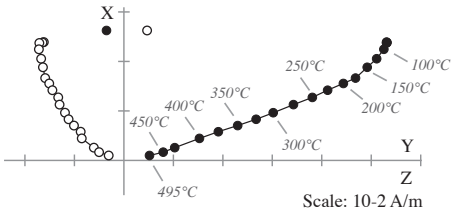

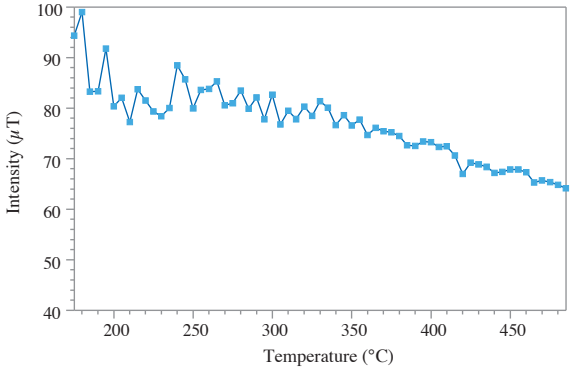

b) SAR13-09A

83.2μT - s=5%

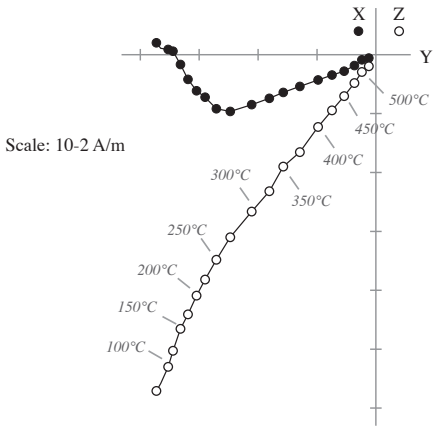

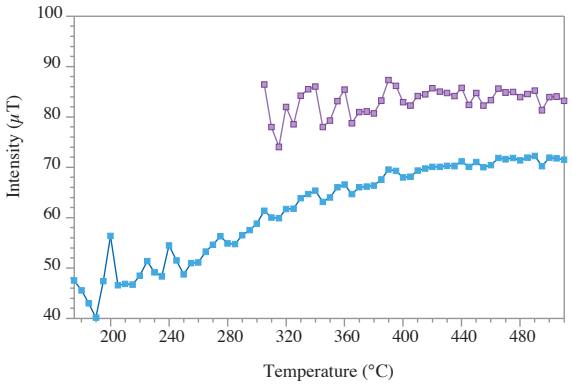

Figure 6

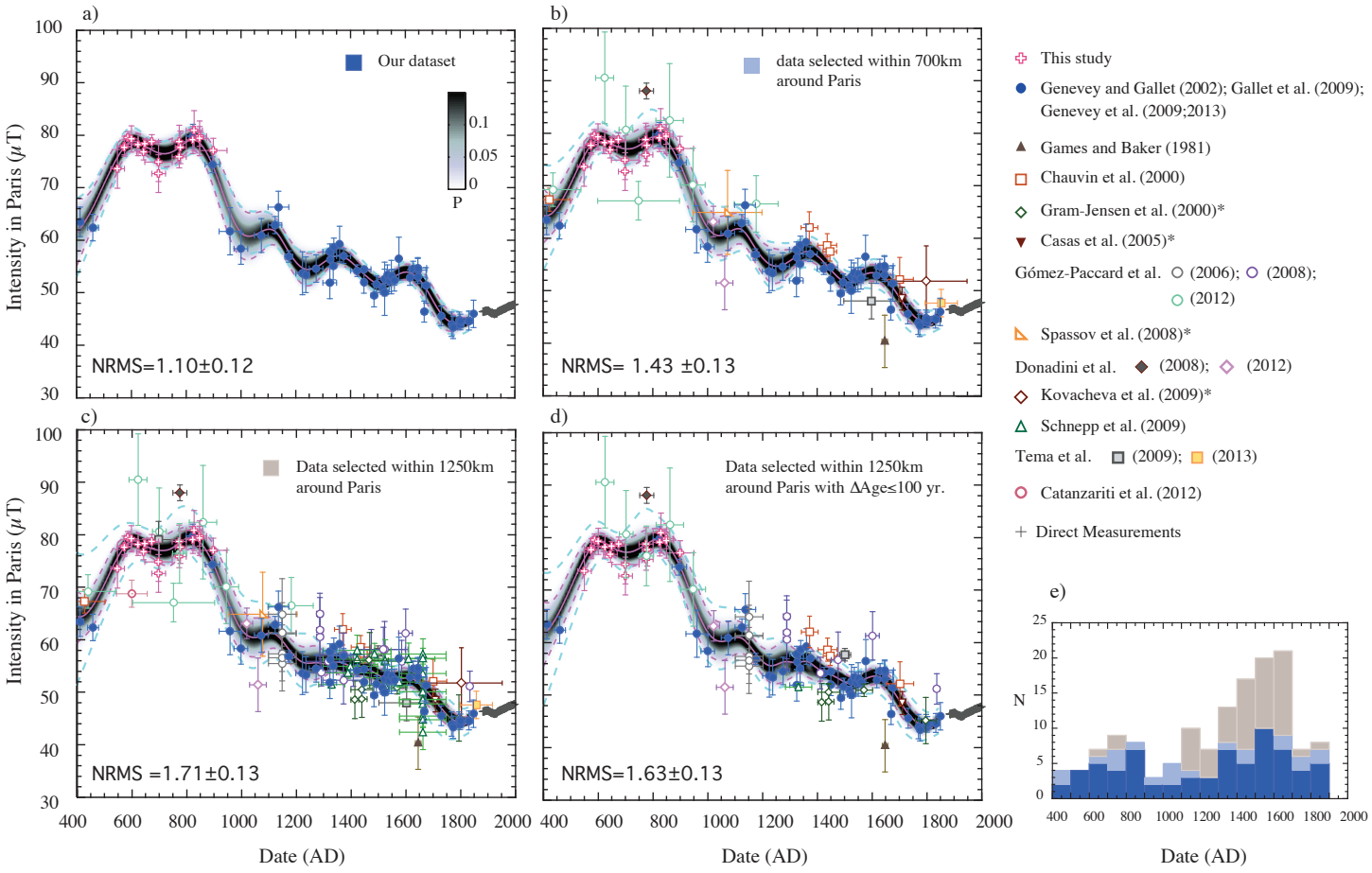
a)
b)
c)
d)
e)
Our dataset
0.1
0.05
0
P
NRMS=1.10±0.12
data selected within 700km around Paris
NRMS= 1.43 ±0.13
Data selected within 1250km around Paris
NRMS =1.71±0.13
Data selected within 1250km around Paris with ΔAge≤100 yr.
NRMS=1.63±0.13
Intensity in Paris (μT)
Date (AD)
N
This study
Genevey and Gallet (2002); Gallet et al. (2009); Genevey et al. (2009;2013)
Games and Baker (1981)
Chauvin et al. (2000)
Gram-Jensen et al. (2000)*
Casas et al. (2005)*
Gómez-Paccard et al. (2006); (2008); (2012)
Spassov et al. (2008)*
Donadini et al. (2008); (2012)
Kovacheva et al. (2009)*
Schnepp et al. (2009)
Tema et al. (2009); (2013)
Catanzariti et al. (2012)
Direct Measurements

Figure 7

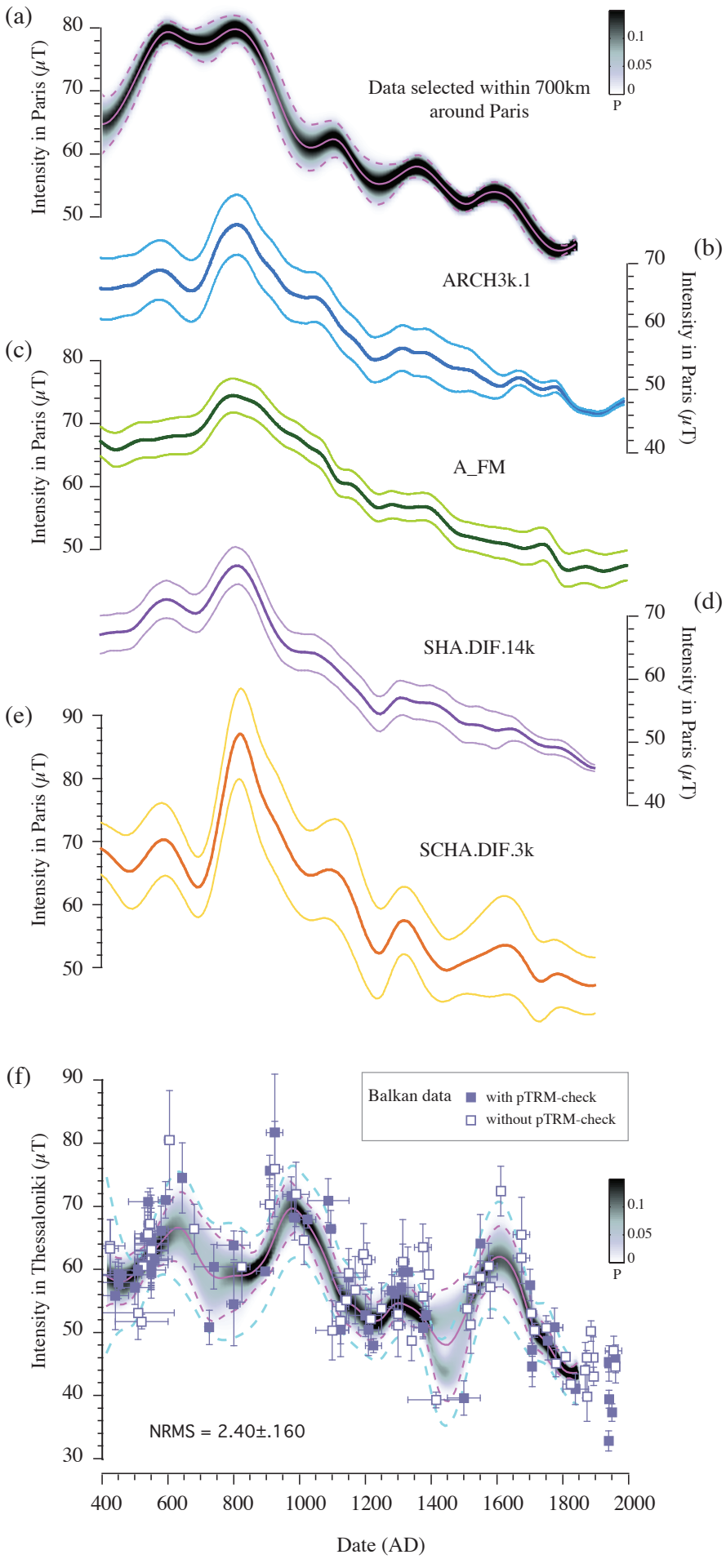
(a)
Intensity in Paris (μT)
Data selected within 700km around Paris
P
(b)
ARCH3k.1
(c)
A_FM
(d)
SHA.DIF.14k
(e)
SCHA.DIF.3k
(f)
Intensity in Thessaloniki (μT)
Balkan data
with pTRM-check
without pTRM-check
NRMS = 2.40±.160
Date (AD)

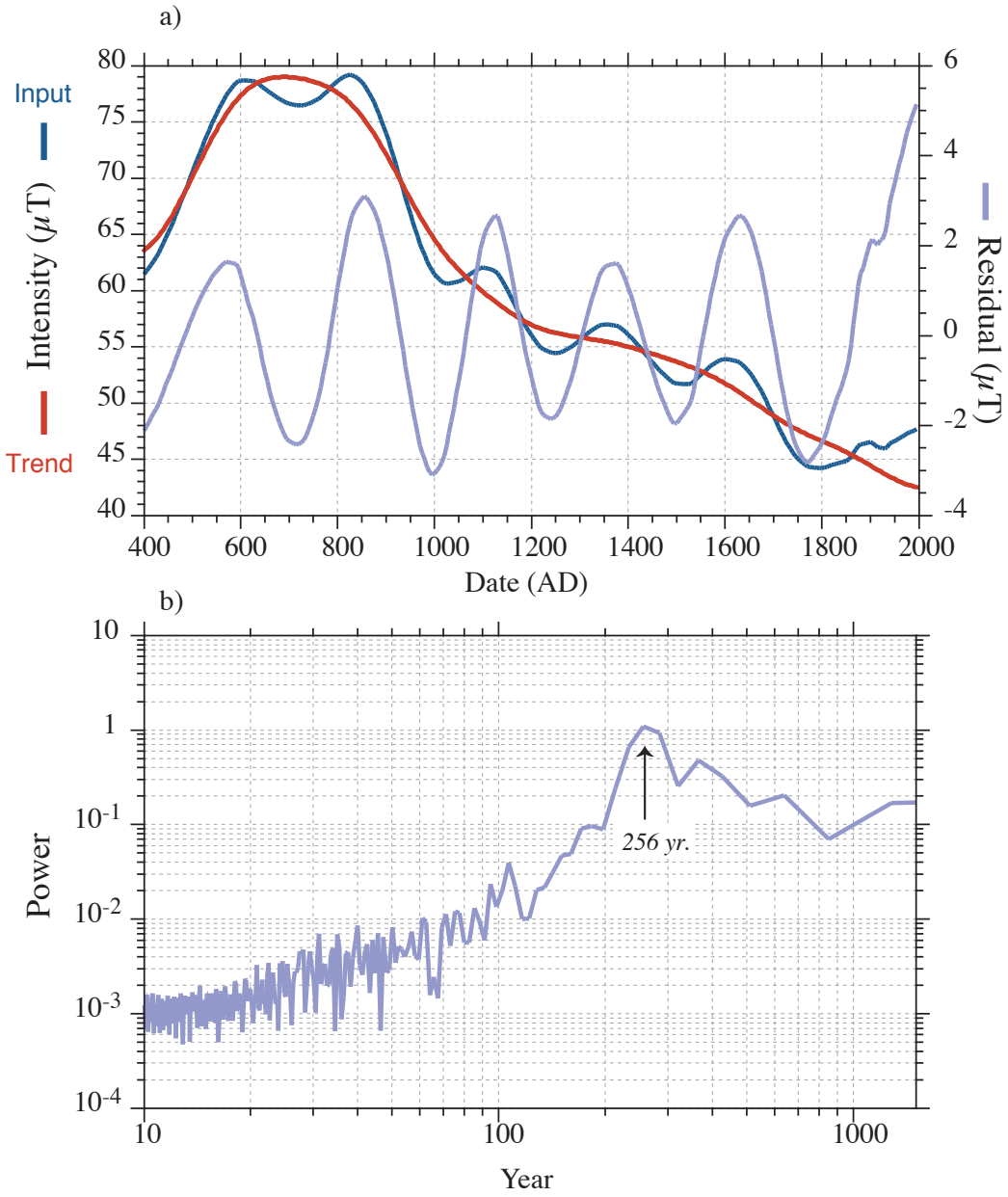
a)
Input
Trend
Intensity (μT)
Residual (μT)
Date (AD)
b)
Power
Year
256 yr.

Figure 9

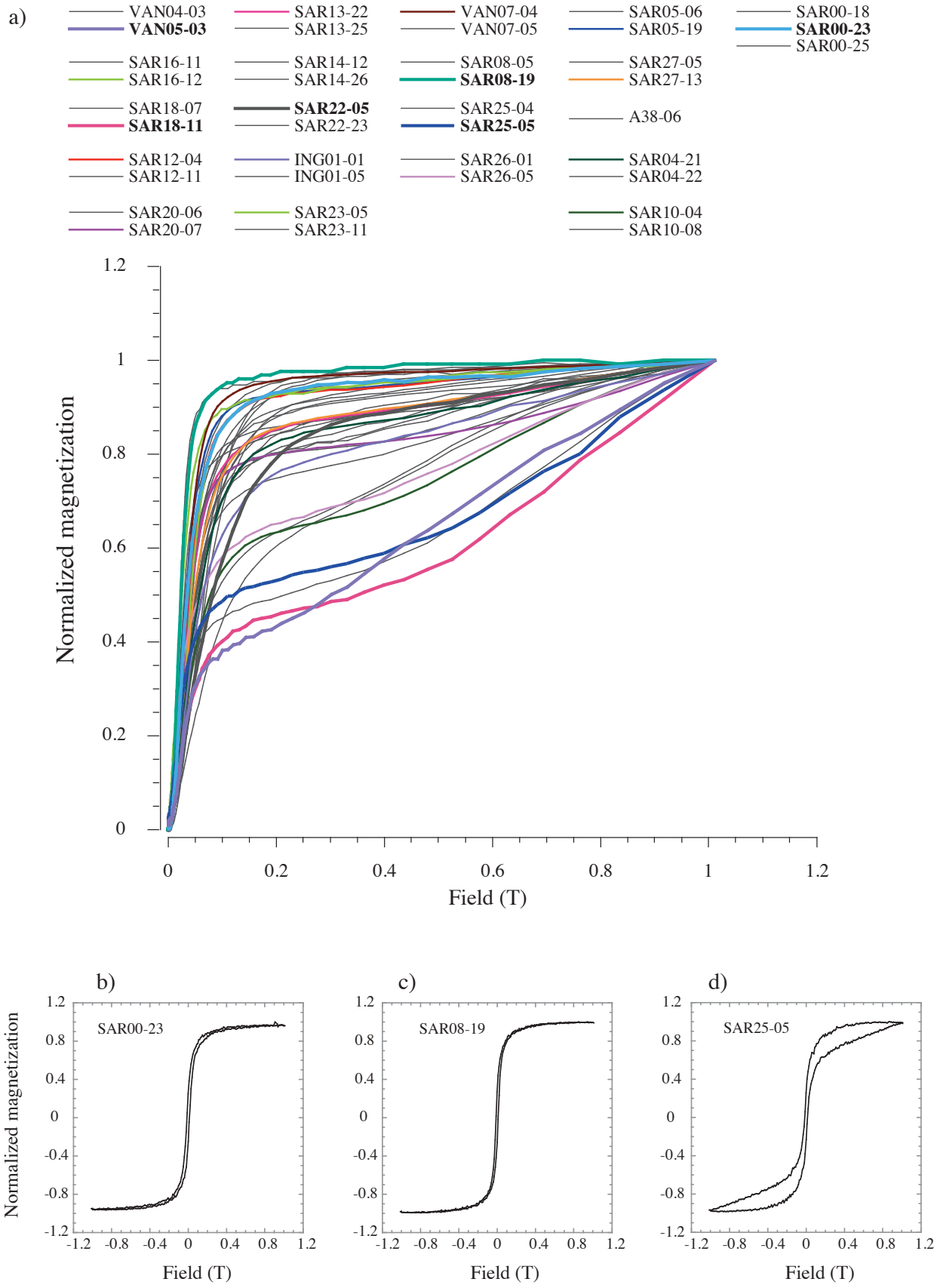
a)
VAN04-03
VAN05-03
SAR13-22
SAR13-25
VAN07-04
VAN07-05
SAR05-06
SAR05-19
SAR00-18
SAR00-23
SAR00-25
SAR16-11
SAR16-12
SAR14-12
SAR14-26
SAR08-05
SAR08-19
SAR27-05
SAR27-13
SAR18-07
SAR18-11
SAR22-05
SAR22-23
SAR25-04
SAR25-05
A38-06
SAR12-04
SAR12-11
ING01-01
ING01-05
SAR26-01
SAR26-05
SAR04-21
SAR04-22
SAR20-06
SAR20-07
SAR23-05
SAR23-11
SAR10-04
SAR10-08
Normalized magnetization
Field (T)
b)
c)
d)
SAR00-23
SAR08-19
SAR25-05
Normalized magnetization
Field (T)

Figure S1

Table 1.

#Group	Age (CE)	Site (Location, Archeological excavation)	Archeological description	N Frag. (n Spec.)	F±σF (μT)	F_{Paris} (μT)
VAN04/VAN05	525-575	Vanves, rue de la République	Pits 2 & 6 (SU 1023 & SU 1039 & SU 2008)	N=4 (n=8)	73.6±1.8	73.6
SAR16	550-600	Saran, Lac de La Médecinerie	Kiln V <=> Kiln 298 (SU 1359)	N=3 (9)	76.9±1.4	77.7
SAR18	550-600	Saran, La Guignace	Pit F313 (SU 1456)	N=8 (n=16)	77.1±1.9	77.9
SAR12	550-600	Saran, Lac de La Médecinerie	Kiln U <=> Kiln 258 (SU 1410)	N=11 (n=22)	78.7±1.2	79.5
SAR20	575-625	Saran, La Guignace	Kiln 7 (SU 3024)	N=8 (n=16)	78.5±2.5	79.3
SAR13	625-675	Saran, Lac de La Médecinerie	Kiln W <=> Kiln 185/186 (SU 1399 & SU 1575)	N=11 (n=22)	77.3±2.6	
SAR14	625-675	Saran, Lac de La Médecinerie	Kiln W <=> Kiln 185/186 (SU 1517)	N=6 (n=12)	77.7±1.1	
SAR13+SAR14	625-675	Saran, Lac de La Médecinerie	Kiln W <=> Kiln 185/186 (SU 1399 & SU 1575 & SU 1517)	N=17 (n=36)	77.4±2.1	78.2
SAR22	625-675	Saran, La Guignace	Kiln 9 (SU 2731)	N=8 (16)	76.1±1.5	76.8
ING01	600-700	Ingré	Pit	N=5 (n=11)	77.6±0.9	78.4
SAR23	650-700	Saran, La Guignace	Kiln 8 (SU 2968)	N=7 (n=14)	78.0±1.3	78.8
VAN07	650-750	Vanves, Rue Gaudray	Kiln 1098 (SU 1128)	N=5 (n=12)	74.9±1.5	74.9
A36/SAR08	675-725	Saran, Zac des Vergers	Kiln 256/2230 (SU 2065 & SU 2066)	N=12 (n=29)	72.0±3.6	72.7
SAR25	750-800	Saran, La Guignace	Kiln 4 (SU 1907)	N=5 (n=10)	78.0±3.1	78.8
SAR26	750-800	Saran, La Guignace	Kiln 11 (SU 1605)	N=4 (n=8)	75.2±2.1	75.9
SAR07	775-825	Saran, Zac des Vergers	Kiln 1148/1242/2319 (SU 10485 & SU 10608)	N=6 (n=12)	76.9±3.1	77.7
SAR05	800-850	Saran, Zac des Vergers	Kiln 2690 (SU 21636 & SU 21637)	N=5 (n=10)	78.3±2.6	79.1
SAR27	800-850	Saran, La Guignace	Kiln 3 (SU 1892)	N=7 (n=14)	80.1±3.8	80.9
A38	800-850	Saran, Lac de La Médecinerie	Kiln E	N=4 (n=12)	79.0±1.9	79.8
SAR04	800-850	Saran, Lac de La Médecinerie	Kiln M <=> Kiln 196 (SU 1467 & SU 1347)	N=10 (n=20)	78.6±3.3	79.4
SAR10	850-950	Saran, le Bourg	Working area	N=4 (n=9)	76.4±2.3	77.1
SAR00	14/11/09	Saran, Lac de La Médecinerie	Experimental firing	N=6 (n=12)	46.6±1.2	47.1

Table 2.

	Our dataset		Data selected within 700 km around Paris	
Date (AD)	**Max. Likelihood (μT)**	**95% Fluctuation Interval (μT)**	**Max. Likelihood (μT)**	**95% Fluctuation Interval (μT)**
400	61.5	6.7	64.4	5.3
425	63.0	5.1	64.5	4.0
450	65.1	4.0	65.8	3.7
475	67.7	3.6	67.8	3.7
500	70.5	3.5	70.4	3.6
525	73.3	3.3	73.1	3.4
550	75.7	2.7	75.7	2.8
575	77.7	2.0	77.8	2.0
600	78.7	1.7	78.9	1.8
625	78.7	1.7	78.8	1.7
650	78.0	1.7	78.1	1.7
675	77.2	1.8	77.4	1.9
700	76.6	2.3	77.1	2.5
725	76.5	2.6	77.1	3.0
750	76.8	2.6	77.7	3.1
775	77.6	2.5	78.6	2.7
800	78.7	2.2	79.4	2.3
825	79.2	2.1	79.4	2.2
850	78.5	2.4	78.6	2.5
875	76.7	3.0	76.8	3.1
900	74.0	3.8	74.2	3.8
925	70.5	4.4	71.1	4.5
950	66.8	4.9	67.7	4.8
975	63.6	5.0	64.6	4.6
1000	61.5	4.7	62.2	4.2
1025	60.6	4.4	60.9	3.8
1050	60.8	4.1	60.6	3.6
1075	61.5	3.8	61.1	3.4
1100	62.0	3.2	61.9	3.0
1125	61.7	2.7	61.8	2.7
1150	60.1	2.4	60.4	2.6
1175	57.9	2.5	58.3	2.8
1200	56.0	2.7	56.5	3.0
1225	54.8	3.1	55.2	3.3
1250	54.4	3.1	54.7	3.3
1275	54.8	2.8	55.0	2.9
1300	55.6	2.2	55.7	2.2
1325	56.5	1.7	56.7	1.7
1350	57.0	1.7	57.5	1.6
1375	56.9	1.8	57.5	1.8
1400	56.1	1.6	56.8	1.7
1425	54.9	1.4	55.6	1.6
1450	53.6	1.4	54.1	1.4
1475	52.5	1.7	52.8	1.6
1500	51.7	1.5	51.8	1.4
1525	51.7	1.1	51.7	1.2
1550	52.5	1.1	52.5	1.1
1575	53.4	1.3	53.2	1.3
1600	53.9	1.5	53.5	1.6
1625	53.7	1.6	53.3	1.5
1650	52.7	1.9	52.4	1.8
1675	51.0	2.4	50.8	2.1
1700	48.8	2.5	48.9	2.4
1725	46.6	2.5	47.1	2.2
1750	45.1	2.1	45.5	1.9
1775	44.3	1.6	44.5	1.6
1800	44.2	1.1	44.2	1.0
1825	44.6	0.7	44.5	0.6
1850	44.8	1.8	45.3	0.9

Table S1.

Potsherd	Samples	n	T_{min}-T_{max}	f	g	q	F_{lab}	F_{non} corrected	σF	F anisotropy corrected	*Genevey and Gallet, 2002*			This study				
											Cooling rate correction factor - Slow cooling time of 10hours from 450°C	*F mean value per potsherd corrected for the cooling rate effect (slow cooling time of 10 hours)*	*F_{mean}±σF (TT-ZI)*	Cooling rate correction factor - Slow cooling time of 4hours from 450°C	F mean value per potsherd corrected for the cooling rate effect (slow cooling time of 4 hours)	F Triaxe mean value per potsherd	F_{mean}±σF (TT-IZ)	F_{mean}±σF (Triaxe)
*A 36 : Saran [675-725 AD]***																		
A36-01	X317	13	150-500	0.89	0.89	51.57	60.0	66.5	1.0	69.5	*0.92*	*62.5±1.7*		0.98	66.5±1.7			
	X318	13	150-500	0.87	0.90	46.39	60.0	65.9	1.1	66.2								
A36-03*	X325	6	375-500	0.62	0.79	19.18	60.0	67.3	1.7	74.7	*X*	*X*		1.00	74.4±0.3	73.9±0.6		
	X326	6	375-500	0.58	0.8	17.48	60.0	64.4	1.7	74.1								
A36-05	X328	11	250-500	0.69	0.90	38.73	60.0	63.4	1.0	69.1	*0.93*	*64.9±0.7*	*63.7±1.1*	0.97	67.7±0.7	68.2±1.1	68.9 ±3.1	71.1±2.9
	X329	12	200-500	0.72	0.91	55.21	60.0	62.7	0.7	70.5								
A36-06	X334	11	250-500	0.81	0.86	45.98	60.0	64.6	1.0	71.7	*0.91*	*64.3±1.0*		0.97	68.6±1.0			
	X335	13	150-500	0.85	0.89	49.74	60.0	61.9	0.9	69.7								
A36-08	X338	14	100-500	0.86	0.90	88.93	60.0	68.9	0.6	69.2	*0.90*	*63.1±0.9*		0.96	67.2±0.9			
	X339	11	250-500	0.80	0.88	62.45	60.0	68.8	0.8	70.9								
*A 38 : Saran [825-875 AD]***																		
A38-02	X250	13	150-500	0.88	0.91	47.41	60.0	83.5	1.4	82.2	*0.93*	*76.1±0.5*		0.99	80.9±0.5			
	X252	13	150-500	0.90	0.91	48.40	60.0	83.8	1.4	81.3								
A38-03*	X253	11	250-500	0.83	0.84	57.20	60.0	74.9	0.9	80.9	*X*	*X*		0.96	79.1±1.5	81.1±0.7		
	X254	11	250-500	0.83	0.84	38.52	60.0	73.2	1.3	83.8								
A38-04	X259	12	200-500	0.88	0.90	49.30	60.0	69.0	1.1	81.8	*0.94*	*77.3±0.4*	*74.7±3.5*	0.95	78.1±0.4		78.0±3.0	80.5±0.6
	X260	11	150-450	0.66	0.88	35.39	60.0	66.6	1.1	82.6								
A38-06	X265	13	150-500	0.82	0.90	44.09	60.0	76.7	1.3	78.2	*0.91*	*70.7±0.5*		0.95	73.8±0.5	79.9±0.4		
	X267	13	150-500	0.81	0.90	43.47	60.0	74.6	1.3	77.2								

Table S2.

Fragment	Specimen	T_{min}-T_{max} (°C)	F Lab (μT)	NRM T1 (T1') (%)	Slope R' (%)	F Triaxe (μT)	F Triaxe mean value per fragment ± σF (μT)
VAN04/05, Vanves, rue de la République, [525-575] AD, (27/17/4)*							
VAN04-03	VAN04-03A	260-505	70	91	-4	73.6	73.2±0.4
	VAN04-03C	270-515	75	90	3	72.8	
VAN04-08	VAN04-08A	210-520	70	87	-1	76.2	75.1±1.1
	VAN04-08C	175-520	75	89	0	74.0	
VAN05-03	VAN05-03A	195-510	75	70	2	74.5	74.8±0.3
	VAN05-03B	180-510	75	81	5	75.0	
VAN05-04	VAN05-04C	260-495	75	67	3	69.7	71.2±1.5
	VAN05-04D	260-485	75	68	1	72.6	
SAR16, Saran, Lac de La Medecinerie, [550-600] AD, (13/7/3)*							
SAR16-06	SAR16-06A	265-510	75	82	-3	77.8	78.5±0.7
	SAR16-06B	225-510	75	90	5	79.1	
	SAR16-06C	270-510	75	89	1	78.2	
SAR16-11	SAR16-11A	195-510	75	87	-3	76.0	76.4±1.1
	SAR16-11B	185-510	75	90	2	77.6	
	SAR16-11C	185-510	75	91	-4	75.5	
SAR16-12	SAR16-12A	205-510	75	94	1	77.5	75.8±1.5
	SAR16-12B	205-510	75	96	1	74.6	
	SAR16-12C	205-510	75	96	5	75.3	
SAR18, Saran, La Guignace, [550-600] AD, (15/9/8)*							
SAR18-01	SAR18-01A	180-490	70	91	3	76.9	75.6±1.3
	SAR18-01B	180-475	75	87	2	74.3	
SAR18-02	SAR18-02A	180-485	70	90	2	75.6	76.7±1.1
	SAR18-02B	220-480	75	85	1	77.7	
SAR18-03	SAR18-03B	200-480	75	93	3	73.7	74.8±1.1
	SAR18-03C	195-480	75	90	0	75.8	
SAR18-07	SAR18-07A	215-485	70	92	3	78.6	79.1±0.5
	SAR18-07B	200-480	75	91	6	79.6	
SAR18-09	SAR18-09A	260-485	70	87	-5	74.0	75.1±1.1
	SAR18-09B	260-480	75	86	0	76.1	
SAR18-10	SAR18-10A	215-490	70	89	3	76.2	77.3±1.1
	SAR18-10B	180-475	75	81	2	78.3	
SAR18-11	SAR18-11A	180-490	70	87	-2	78.5	78.5±0.0
	SAR18-11B	180-475	75	84	1	78.5	
SAR18-14	SAR18-14A	205-490	70	86	-3	79.7	79.7±0.0
	SAR18-14B	205-490	75	83	1	79.7	
SAR12, Saran, Lac de La Medecinerie, [550-600] AD, (27/16/11)*							
SAR12-02	SAR12-02A	230-510	80	84	4	76.7	77.5±0.8
	SAR12-02B	235-505	75	89	1	78.3	
SAR12-03	SAR12-03A	175-505	65	93	3	79.6	79.9±0.3
	SAR12-03B	195-495	75	73	9	80.1	
SAR12-04	SAR12-04A	175-505	80	93	-3	76.2	76.5±0.3
	SAR12-04B	205-495	75	94	6	76.7	
SAR12-06	SAR12-06A	195-510	80	93	1	78.2	78.9±0.7
	SAR12-06B	195-485	75	93	2	79.5	

SAR12-11	SAR12-11A	175-505	75	89	2	78.6	78.4±0.2
	SAR12-11B	175-505	75	84	3	78.2	
SAR12-15	SAR12-15B	180-495	75	91	5	77.9	77.4±0.5
	SAR12-15C	180-495	75	93	7	76.9	
SAR12-17	SAR12-17A	175-495	75	93	-1	80.7	80.6±0.2
	SAR12-17B	175-490	75	93	-3	80.4	
SAR12-18	SAR12-18A	175-505	75	87	3	79.6	79.8±0.2
	SAR12-18B	175-505	75	91	-2	80.0	
SAR12-21	SAR12-21A	175-505	75	95	7	78.9	79.0±0.1
	SAR12-21B	175-505	75	89	9	79.0	
SAR12-25	SAR12-25A	175-505	75	96	-2	79.0	78.5±0.5
	SAR12-25B	175-500	75	96	7	77.9	
SAR12-27	SAR12-27A	175-505	75	81	5	78.9	79.1±0.2
	SAR12-27B	200-505	75	78	6	79.3	

SAR20, Saran, La Guignace, [575-625] AD, (16/14/8)*

SAR20-03	SAR20-03A	185-485	75	88	-2	76.2	77.2±1.0
	SAR20-03B	200-485	75	84	-4	78.2	
SAR20-04	SAR20-04A	240-485	75	86	-1	81.3	81.3±0.1
	SAR20-04B	240-475	75	79	4	81.2	
SAR20-06	SAR20-06A	180-490	75	86	4	75.2	76.0±0.8
	SAR20-06B	180-475	75	80	-2	76.7	
SAR20-07	SAR20-07A	180-485	75	91	-2	77.9	79.4±1.5
	SAR20-07B	180-475	75	89	-2	80.8	
SAR20-09	SAR20-09A	180-485	75	87	0	78.3	78.2±0.2
	SAR20-09B	190-475	75	78	-4	78.0	
SAR20-10	SAR20-10A	225-485	75	80	-6	75.9	76.2±0.3
	SAR20-10B	230-485	75	80	1	76.4	
SAR20-14	SAR20-14A	255-485	75	85	0	83.0	83.0±0.0
	SAR20-14B	275-475	75	80	4	83.0	
SAR20-15	SAR20-15A	175-475	75	79	0	76.5	76.9±0.4
	SAR20-15B	175-475	75	79	2	77.2	

SAR13, Saran, Lac de La Medecinerie, [625-675] AD, (27/21/11)*

SAR13-04	SAR13-04A	180-500	75	90	5	79.8	78.3±1.5
	SAR13-04B	180-495	75	91	3	76.8	
SAR13-08	SAR13-08A	340-505	75	94	4	81.5	80.8±0.8
	SAR13-08C	375-510	75	90	4	80.0	
SAR13-09	SAR13-09A	305-510	75	75	5	83.2	83.3±0.1
	SAR13-09B	325-495	75	84	3	83.3	
SAR13-13	SAR13-13A	175-510	75	90	-5	76.0	75.6±0.6
	SAR13-13D	180-510	75	91	-3	75.1	
SAR13-14	SAR13-14A	245-510	75	92	5	74.1	75.2±1.1
	SAR13-14B	250-500	75	87	5	76.3	
SAR13-16	SAR13-16A	220-510	75	95	6	77.0	76.9±0.2
	SAR13-16C	225-500	75	91	1	76.7	
SAR13-18	SAR13-18A	205-510	75	90	5	75.4	76.3±0.9
	SAR13-18B	225-500	75	91	5	77.2	
SAR13-19	SAR13-19A	220-510	75	92	2	76.2	75.8±0.4
	SAR13-19B	180-500	75	85	-4	75.4	
SAR13-20	SAR13-20B	200-495	75	96	-1	76.4	76.3±0.2
	SAR13-20C	200-485	75	93	1	76.1	
SAR13-22	SAR13-22A	175-500	75	95	3	77.3	77.3±0.0
	SAR13-22B	200-500	75	94	-1	77.3	
SAR13-25	SAR13-25A	175-490	75	94	2	73.7	74.9±1.2
	SAR13-25B	185-490	75	89	6	76.0	

SAR14, Saran, Lac de La Medecinerie, [625-675] AD, (27/11/6)*

SAR14-03	SAR14-03A	230-490	75	79	1	78.3	78.1±0.3
	SAR14-03B	215-505	75	89	2	77.8	
SAR14-07	SAR14-07A	175-505	75	95	4	77.8	77.4±0.4
	SAR14-07B	175-485	75	91	8	77.0	
SAR14-09	SAR14-09A	175-505	75	89	7	76.8	77.4±0.6
	SAR14-09B	175-490	75	93	5	78.0	
SAR14-12	SAR14-12A	175-490	75	95	4	75.9	76.2±0.3
	SAR14-12B	175-485	75	91	2	76.4	
SAR14-19	SAR14-19A	220-505	75	93	1	79.1	79.4±0.3
	SAR14-19B	245-490	75	93	1	79.7	
SAR14-26	SAR14-26A	175-505	75	89	0	77.4	77.4±0.1
	SAR14-26C	200-510	75	91	1	77.3	

SAR22, Saran, La Guignace, [625-675] AD, (23/14/8)*

SAR22-05	SAR22-05A	180-490	75	91	5	75.4	74.2±1.3
	SAR22-05B	180-495	75	88	6	72.9	
SAR22-08	SAR22-08A	415-490	75	79	-2	77.2	76.8±0.4
	SAR22-08B	340-480	75	81	0	76.4	
SAR22-10	SAR22-10A	250-495	75	91	2	76.3	76.6±0.3
	SAR22-10B	245-490	75	87	4	76.9	
SAR22-11	SAR22-11A	200-490	75	90	2	79.1	78.9±0.2
	SAR22-11B	180-485	75	89	1	78.7	
SAR22-12	SAR22-12A	250-485	75	84	4	78.1	77.0±1.1
	SAR22-12B	265-485	75	92	6	75.9	
SAR22-17	SAR22-17A	180-485	75	91	0	75.0	74.9±0.2
	SAR22-17B	180-480	75	87	-3	74.7	
SAR22-21	SAR22-21A	175-485	75	90	2	76.0	75.3±0.7
	SAR22-21B	180-480	75	86	2	74.6	
SAR22-23	SAR22-23A	200-490	75	93	4	75.1	75.0±0.2
	SAR22-23B	180-480	75	88	1	74.8	

ING01, Ingré, [600-700] AD, (11/10/5)*

ING01-01	ING01-01A	180-515	80	86	2	79.0	78.7±0.5
	ING01-01B	175-500	80	89	-3	78.1	
	ING01-01C	175-495	80	87	3	79.0	
ING01-04	ING01-04A	200-495	80	79	1	77.8	77.2±0.6
	ING01-04B	180-490	75	93	6	76.6	
ING01-05	ING01-05A	175-515	80	92	-3	76.3	76.5±0.2
	ING01-05C	175-495	75	86	-6	76.6	
ING01-07	ING01-07A	200-455	70	96	-1	79.5	78.4±1.1
	ING01-07B	175-475	80	94	4	77.3	
ING01-09	ING01-09A	200-460	75	69	-2	78.1	77.1±1.0
	ING01-09C	195-480	75	76	2	76.1	

SAR23, Saran, La Guignace, [650-700] AD, (17/15/7)*

SAR23-04	SAR23-04A	215-490	75	83	4	78.2	77.7±0.6
	SAR23-04C	175-482	75	89	0	77.1	
SAR23-05	SAR23-05A	195-485	75	83	5	78.2	78.6±0.4
	SAR23-05B	205-490	75	88	1	79.0	
SAR23-06	SAR23-06A	175-485	75	83	1	77.7	78.5±0.8
	SAR23-06B	180-485	75	82	-1	79.3	
SAR23-09	SAR23-09A	180-490	75	83	4	75.2	76.0±0.8
	SAR23-09B	190-485	75	83	-1	76.8	
SAR23-15	SAR23-15A	200-490	75	92	4	76.6	76.8±0.2

	SAR23-15B	180-490	75	92	2	76.9	
SAR23-16	SAR23-16A	180-485	75	89	2	79.4	79.9±0.5
	SAR23-16B	180-490	75	89	1	80.4	
SAR23-17	SAR23-17A	225-490	75	88	4	76.9	78.2±1.3
	SAR23-17B	260-485	75	77	6	79.4	

VAN07, Vanves, Rue Gaudray, [650-750] AD, (14/13/5)*

VAN07-04	VAN07-04A	220-500	75	93	7	75.4	75.6±0.3
	VAN07-04B	175-490	75	91	3	75.5	
	VAN07-04C	240-490	75	88	5	76.0	
VAN07-05	VAN07-05A	175-500	75	91	-3	74.2	73.1±1.1
	VAN07-05B	175-500	75	90	4	72.0	
VAN07-06	VAN07-06A	175-500	75	86	-4	76.4	76.7±1.3
	VAN07-06B	225-490	75	73	4	78.1	
	VAN07-06C	255-500	75	79	8	75.5	
VAN07-08	VAN07-08A	250-500	75	89	7	75.2	75.7±0.5
	VAN07-08B	250-500	75	94	5	76.1	
VAN07-09	VAN07-09A	185-500	75	86	1	74.5	73.6±1.0
	VAN07-09B	195-500	75	88	7	72.6	

A36/SAR08, Saran, Zac des Vergers, [675-725] AD, (43/29/9)*

A36-03	A36-03C	380-520	70	89	0	74.5	73.9±0.6
	A36-03D	360-520	70	87	1	73.3	
A36-05	A36-05A	390-485	65	69	6	69.3	68.2±1.1
	A36-05C	355-500	70	80	4	67.1	
SAR08-05	SAR08-05B	205-485	70	87	6	75.5	73.8±1.7
	SAR08-05C	180-480	70	91	2	72.1	
SAR08-13	SAR08-13A	335-480	70	79	4	72.3	72.5±0.2
	SAR08-13C	385-495	70	77	-3	72.7	
SAR08-18	SAR08-18A	180-515	70	94	-1	75.9	76.7±0.8
	SAR08-18B	185-500	70	92	2	77.4	
SAR08-19	SAR08-19A	225-500	70	96	4	71.0	71.4±0.4
	SAR08-19C	265-495	70	95	5	71.7	
SAR08-23	SAR08-23A	250-500	70	96	5	74.7	74.6±0.5
	SAR08-23B	240-470	70	86	4	74.1	
	SAR08-23C	205-465	70	80	5	75.1	
SAR08-33	SAR08-33A	215-500	70	91	3	72.6	72.9±0.3
	SAR08-33B	235-470	70	77	3	73.1	
SAR08-34	SAR08-34A	195-500	70	98	4	76.6	77.0±0.4
	SAR08-34B	225-470	70	83	2	77.4	

SAR25, Saran, La Guignace, [750-800] AD, (9/9/5)*

SAR25-01	SAR25-01A	175-495	75	90	2	80.2	80.2±0.1
	SAR25-01B	190-485	75	86	2	80.1	
SAR25-02	SAR25-02A	195-495	75	91	-3	73.2	73.5±0.3
	SAR25-02B	176-495	75	89	-1	73.8	
SAR25-04	SAR25-04A	175-500	75	94	3	79.4	79.4±0.0
	SAR25-04B	175-485	75	90	4	79.4	
SAR25-05	SAR25-05A	175-495	75	89	2	75.2	76.0±0.8
	SAR25-05B	175-485	75	87	-6	76.7	
SAR25-06	SAR25-06A	175-495	75	85	0	81.1	80.8±0.4
	SAR25-06B	175-485	75	91	1	80.4	

SAR26, Saran, La Guignace, [750-800] AD, (12/8/4)*

SAR26-01	SAR26-01A	175-495	75	98	4	73.2	73.3±0.1
	SAR26-01B	175-490	75	96	1	73.3	

SAR26-02	SAR26-02A	180-500	75	94	0	73.4	74.2±0.8
	SAR26-02B	175-490	75	91	-1	74.9	
SAR26-06	SAR26-06B	225-520	75	94	5	75.0	75.0±0.0
	SAR26-06C	225-520	75	94	4	75.0	
SAR26-08	SAR26-08A	270-485	75	75	5	78.0	78.2±0.2
	SAR26-08B	280-500	75	85	7	78.4	
SAR07, Saran, Zac des Vergers, [775-825] AD, (30/23/6)*							
SAR07-01	SAR07-01B	195-515	75	83	0	78.4	77.4±1.0
	SAR07-01C	175-530	75	90	-3	76.4	
SAR07-10	SAR07-10A	320-485	75	85	2	71.6	70.9±0.8
	SAR07-10B	355-480	75	85	-3	70.1	
SAR07-19	SAR07-19A	175-500	75	93	-3	79.6	80.0±0.4
	SAR07-19B	175-480	75	88	-2	80.3	
SAR07-21	SAR07-21A	255-505	75	94	-4	77.6	78.1±0.5
	SAR07-21B	255-480	75	83	5	78.5	
SAR07-23	SAR07-23A	175-500	75	93	1	78.2	78.2±0.0
	SAR07-23B	175-485	75	85	-2	78.2	
SAR07-26	SAR07-26A	230-480	75	82	3	75.2	77.0±1.8
	SAR07-26B	270-470	75	75	2	78.7	
SAR05, Saran, Zac des Vergers, [800-850] AD, (24/22/5)*							
SAR05-03	SAR05-03B	345-540	80	96	-2	77.8	78.3±0.5
	SAR05-03D	310-540	80	91	3	78.7	
SAR05-06	SAR05-06A	175-515	80	96	-4	82.4	82.8±0.4
	SAR05-06B	175-490	80	83	-1	83.1	
SAR05-11	SAR05-11A	175-520	80	94	-6	75.4	76.3±0.9
	SAR05-11B	175-485	80	85	-2	77.1	
SAR05-13	SAR05-13A	310-515	80	80	0	78.4	77.2±1.2
	SAR05-13C	335-505	80	83	-2	76.0	
SAR05-19	SAR05-19A	180-480	80	88	4	77.1	77.0±0.1
	SAR05-19B	175-470	80	82	1	76.9	
SAR27, Saran, La Guignace, [800-850] AD, (14/14/7)*							
SAR27-01	SAR27-01A	175-495	80	86	-3	79.8	78.7±1.1
	SAR27-01B	175-495	80	88	7	77.6	
SAR27-03	SAR27-03A	190-475	80	93	0	80.8	79.0±2.0
	SAR27-03B	175-475	80	87	5	77.1	
SAR27-05	SAR27-05A	295-495	80	81	2	83.2	82.8±0.4
	SAR27-05C	280-495	80	76	2	82.4	
SAR27-07	SAR27-07A	335-495	80	82	0	74.0	74.1±0.1
	SAR27-07B	335-495	80	83	1	74.1	
SAR27-09	SAR27-09B	175-510	80	87	-1	81.5	81.8±0.3
	SAR27-09C	190-510	80	87	0	82.0	
SAR27-10	SAR27-10A	235-495	80	90	7	77.4	78.1±0.7
	SAR27-10B	200-485	80	87	4	78.8	
SAR27-13	SAR27-13A	290-495	80	65	5	86.3	86±0.4
	SAR27-13B	325-520	80	76	7	85.6	
A38, Saran, Lac de La Medecinerie, [800-850] AD, (6/5/2)*							
A38-03	A38-03B	295-505	80	97	7	81.8	81.1±0.7
	A38-03C	255-510	80	97	6	80.4	
A38-06	A38-06B	175-470	80	92	1	79.5	79.9±0.4
	A38-06B	175-465	80	89	2	80.2	
SAR04, Saran, Lac de La Medecinerie, [800-850] AD, (31/26/10)*							

SAR04-03	SAR04-03A	295-495	80	88	-1	73.4	74.1±0.7
	SAR04-03B	280-475	75	88	5	74.7	
SAR04-13	SAR04-13A	333-495	80	81	3	75.4	75.4±0.0
	SAR04-13B	310-490	75	90	4	75.4	
SAR04-17	SAR04-17A	175-495	80	79	-3	79.2	79.0±0.2
	SAR04-17B	175-475	75	78	-4	78.8	
SAR04-18	SAR04-18A	175-480	75	89	1	82.0	81.5±0.5
	SAR04-18C	175-500	75	88	5	81.0	
SAR04-19	SAR04-19A	360-480	75	75	-6	83.5	82.3±1.2
	SAR04-19B	400-470	75	63	2	81.1	
SAR04-21	SAR04-21A	180-480	75	87	9	80.1	81.3±1.2
	SAR04-21B	200-470	75	78	3	82.5	
SAR04-22	SAR04-22A	240-480	75	81	6	77.6	76.9±0.8
	SAR04-22B	260-485	75	91	6	76.1	
SAR04-24	SAR04-24A	175-480	75	72	0	82.9	83.1±0.2
	SAR04-24B	180-490	75	87	-3	83.2	
SAR04-25	SAR04-25A	245-480	75	83	6	76.6	76.7±0.1
	SAR04-25B	270-480	75	82	6	76.7	
SAR04-29	SAR04-29A	220-480	75	92	6	75.0	75.5±0.5
	SAR04-29B	225-485	75	91	5	75.9	
SAR10, Saran, le Bourg, [850-950] AD, (9/7/4)*							
SAR10-03	SAR10-03A	225-490	75	90	9	73.6	74.1±0.5
	SAR10-03B	225-470	75	87	3	74.1	
	SAR10-03C	225-460	75	82	5	74.5	
SAR10-04	SAR10-04A	335-490	75	78	-1	79.6	79.3±0.4
	SAR10-04C	325-500	75	91	4	78.9	
SAR10-05	SAR10-05A	175-490	75	96	6	75.9	75.2±0.8
	SAR10-05C	175-460	75	86	-1	74.4	
SAR10-08	SAR10-08B	195-490	75	83	6	76.9	76.9±0.0
	SAR10-08C	175-490	75	86	8	76.9	
SAR00, Saran, Lac de La Medecinerie, 14/11/2009, (17/6/6)*							
pot 10	SAR00-10A	185-495	50	80	-3	48.1	47.4±0.7
	SAR00-10B	195-495	50	79	-5	46.7	
pot 18	SAR00-18A	210-495	50	72	-8	47.0	47.3±0.3
	SAR00-18B	185-490	50	72	1	47.5	
pot 23	SAR00-23A	220-495	50	90	1	43.0	44.1±1.1
	SAR00-23B	200-485	50	89	0	45.1	
pot 25	SAR00-25A	190-485	50	67	-2	47.9	47.0±0.9
	SAR00-25B	195-510	50	78	-6	46.1	
pot 36	SAR00-36A	190-495	50	86	2	47.2	46.7±0.5
	SAR00-36B	195-510	50	92	-4	46.2	
pot 48	SAR00-48A	180-510	50	91	-4	46.8	46.8±0.0
	SAR00-48B	180-495	50	84	-6	46.8	